ELECTRICAL DETECTION OF SINGLE-BASE DNA MUTATION USING FUNCTIONALIZED NANOPARTICLES

by

MOHAMMUD R. NOOR

Presented to the Faculty of the Graduate School of

The University of Texas at Arlington in Partial Fulfillment

of the Requirements

for the Degree of

MASTER OF SCIENCE IN ELECTRICAL ENGINEERING

THE UNIVERSITY OF TEXAS AT ARLINGTON

December 2009

ACKNOWLEDGEMENTS

First, I would like to thank my mentor and advisor Dr. Samir M. Iqbal for his unwavering support and patience since I started my graduate school. I am deeply impressed by the depth of his knowledge and enthusiasm in Bio-Nanotechnology. His passion for science and relentless desire to create novel approaches in disease diagnostics inspired me profoundly. I really appreciate his help in every step of the way. I feel extremely honored to have Dr. Zynep Celik Butler and Dr. Dereje Agonafer in my master's advisory committee. I want to thank Dr. Zynep Celik Butler for her important feedback in my thesis.

My special thanks go to all my lab mates that I worked with for more than two years. I really want to acknowledge the support of two of my lab mates, Swati Goyal and Priyanka Ramachandran. I also want to thank all the Nanofab staffs such as Eduardo Maldonado, Dennis Bueno, Fatima Amir and Paul Logan for their training and kind help whenever I needed it the most.

I also want to thank all my friends and family for their prayers and well wishes. Without their prayers and grace of all Mighty Allah I would not be able to accomplish this feat. My Mom and Dad, siblings and close friends, all have important contributions to my success. Last but not least, I want to thank my fiancé Sharmin Taher for her excellent support, especially at my bad times. I knew she was always by my side which gave me courage and inspiration to carry on at tough times.

December 2, 2009

ABSTRACT

ELECTRICAL DETECTION OF SINGLE-BASE DNA MUTATION USING FUNCTIONALIZED NANOPARTICLES

Mohammud R. Noor, M.S

The University of Texas at Arlington, 2009

Supervising Professor: Samir M. Iqbal

DNA molecules possess unique structure and molecular recognition properties that makes them excellent candidate for bio-chemical sensors. Understanding the mechanism of charge transport in DNA is essential to develop DNA based molecular electronic devices. In the experiment reported in this thesis, we analyzed an electrical method to detect specific DNA. Hairpin probe DNA was engineered to melt and hybridize with certain perfect complementary sequences and immobilized on a silicon chip between gold nanoelectrodes. Hybridization of target DNA to the hairpin melts or open up the stem nucleotides, which provides DNA hybridization sites. Gold nanoparticle-conjugated universal reporter sequence detects the open sites of hairpins by annealing to the exposed stem nucleotides. The gold nanoparticles along with the DNA facilitate the movement of electrons, hence increasing the charge conduction between the electrodes. Specifically, we used a hairpin probe designed to detect a medically relevant mutant form of the *K*-Ras oncogene. Direct *I-V* measurements of the nanoelectrodes both before and after the DNA attachment showed three orders of magnitude increase in conductivity for as low as 2 fmol of target molecules.

TABLE OF CONTENTS

LIST OF ILLUSTRATIONS

LIST OF TABLES

Table Page

CHAPTER 1

INTRODUCTION

Charge conduction in DNA has introduced a new approach in molecular electronics which is rapidly gaining momentum in miniaturizing electronics components [1]. The properties of individual molecules and DNA have been used to perform the functions of traditional components (transistors, diodes, wires, etc). The motivation behind this research work and thesis is directly derived from molecular electronics and relevant bio-chemical sensor field. The research to date has found DNA as an excellent carrier for charge transport because of π-stacking of base pairs in its double-helix structure. The main goal of this thesis work is to show how the melting and hybridization of hairpin loop DNA with perfect complimentary and single base pair mismatch DNA changes the charge transport through them, thus making electrical detection possible. These distinct characteristics can be implemented as very sensitive bio-chemical sensor. In this thesis, the importance of DNA molecular electronics and its relevance with nanotechnology, different fabrication methods, different mechanisms of charge transport in DNA and the implementation of this new technology in making ultra sensitive bio-sensors have been briefly discussed.

The study of the properties of DNA and its charge conductive nature has been made possible by the advancement in nanotechnology. In Chapter 3, the different techniques used for measuring the electrical conductivity of DNA were briefly discussed. These will include the break junction method, nanoelectrode-gap method, self assembled nanojunction method and other state-of-the art methods. Almost all of those techniques were successfully employed by many researchers to study the electrical properties of DNA. In different experiments, researchers have found that DNA behaves with a contrasting nature of a conductor, a

semiconductor, or an insulator. However, recent research tends to prove the conductive nature of DNA. Also in Chapter 3, few of these experiments were shown and an effort was made to arbitrate these contradictory results, showing how the factors such as base sequence, counterions, length and ambient conditions can affect the charge conduction of DNA.

Nano-gap based sensors are a very new concept but rapidly gaining more significance in diverse areas of bio-medical field. Nanotechnology based sensors are replacing many conventional sensor systems because of their minute size but huge functionality and high reliability. Sensor performance largely depends on properties such as the sensitivity, hysteresis, lifetime, cost and range of operation. The primary focus of this thesis is on nano-junction based sensor, and its application on sensor field using the electrical transport properties through individual molecule for the characterization of DNA. DNA has long been a candidate for such devices [2], only now the emerging break junction sensors are making the use of it. These kinds of sensors can have wide applications in molecular electronics and a new approach to look at more advanced biological sensors.

Standard chemical and biological sensors that are used nowadays do have some limitations and drawbacks [3]. In the field of biomedical engineering, advance detection of minute particles, cell mutation or characterization of one to few hundreds of DNA molecules are still a huge problem. Most sensors employed in bio-chemical detection require a large amount or high concentration of samples (usually millions of cells) to measure considerable amount of change in them, which in turn detects a disease, bacteria or virus. In few cases, the presence of high concentration of target molecules in human means the disease is in advanced stage and it's already too late to cure it. Standard biochemical sensors based on direct or indirect DNA electrochemistry suffer from many disadvantages such as contamination of samples, ambient conditions and expiration time of samples [3], which decreases the potential of quick diagnosis of a certain sample. In practice, many different types of chemical and biological sensors are in use which are very specific in detecting a particular target molecule in a specimen. Even though

recent technologies and research do not lead to one universal sensor, but it is possible to widen the field of a sensor to analyze different types of target in a given specimen. So it is a necessity for a sensor that can perform in wide range of conditions to give exact specimen information. Based on the famous description of electronic transport through individual molecule [4], numerous experiments and researches have been carried out on DNA and its electrical properties [2]. In such experiments, DNA was used as a "fuse" and the electrical conduction through it was reported [5-9]. The goal is to device a sensory system with the help of nano gap break-junction by electromigration through thin gold-on-titanium films. Following the same experimental procedure reported earlier [10], the system can record the resistances of all the samples used as a fuse in a nano-gap break junction. The effect of temperature ramping and subsequently different conductance of the same sample can be recorded and used to analyze the sample. It is strongly believed that the proposed system and its findings can have important consequences in DNA-based molecular electronics and direct label-free detection of DNA hybridization.

1.1 Molecular Electronics

For more than 40 years now, the semiconductor industry has been driven to catch up with the predictions of Moore's Law. Moore's Law basically states that the number of transistors on an integrated circuit will be doubled in about every 24 months. Intel has been successful to keep the pace of its co-founder's trend for more than 40 years. Recently Intel introduced the 32 nm chip technology by using high-*k* dielectric and immersion lithography on 'critical layers', meaning that a refractive fluid will fill the gap between the lens and the wafer during the fabrication process. AMD is already using immersion lithography to make its 45 nm CPUs, but Intel has so far used dry lithography on its 45 nm CPUs [11]. However, the laws of physics suggest that this doubling cannot continue forever. Eventually, the transistors will become so tiny that their silicon components will approach the size of molecules. At these incredibly tiny distances, the complicated rules of quantum mechanics take over, permitting electrons to jump

from one place to another without passing through the space in between. This way, the gate potential would not be able to control the switching of current, and the whole device will fail. Also, conventional lithographic methods are not useful to fabricate integrated circuits that will follow Moore's Law indefinitely. This is where the idea of molecular electronics can play a vital role and has been proposed widely by using a "bottom-up" approach to solve this problem. Similarly, molecular electronics can also lead the field of bio-chemical sensors with its unique approach towards signal sensing and information processing. In this chapter, the need of molecular electronics in bio-chemical sensor technology and its potential advantages will be discussed. Next, a brief explanation will be provided about different kind of bio-chemical sensors conventionally used, followed by the introduction of several components of molecular electronics, such as gold nanoparticles, carbon nanotubes, self-assembled monolayer and DNA molecules. The properties and structures of the hairpin loop DNA will also be duscussed, especially for the ones used in the work of this thesis. Finally in this chapter, a detailed description of the charge transport mechanisms in DNA which enable long distance charge transfer, such as thermal hopping, coherent tunneling and diffusive tunneling will be given.

1.2 Importance of Molecular Electronics in Bio-Chemical Detection

To keep pace with Moore's law, the electronics industry is in a relentless pursuit to fabricate smaller devices and to accommodate more components (transistors, resistors, capacitors and wires) on a single chip. Conventionally, a top down lithographic approach have been followed so far. Most of these lithographic techniques use light, and the problem arises when the device gets smaller than the wavelength of light itself. This problem restricts the process of miniaturizing of circuits to a resolution of tens of nanometers [12]. To cope up with the demand of semiconductor industry, new lithographic processes such as electron beam lithography and immersion lithography have emerged and have successfully overcome the problem with a certain size limit. Since 2006, devices with features of 32 nm have been demonstrated using photolithography [13] and chips with 65 nm features are commercially

available using these new lithographic processes. As the number of components on a single chip increases dramatically, the amount of power dissipation also increases [14]. When the sizes of the components are scaled down to nanometers and beyond, they loose their natural properties and start showing different behavior. The valence and conduction bands break up into discrete energy levels, and eventually change the basic concept of electron-transport mechanism in circuits. So at this incredibly miniature level, it is really necessary to develop conceptually new devices to overcome the limitations of the top-down approach of semiconductor electronic devices fabrication.

The visionary lecture by Richard P. Feynman presented on December 29th, 1959, did set up the stepping stone for Nanotechnology and gave inspiration for electronic components made of individual atoms and molecules [15]. Dr. Feynman was especially interested on diversifying the general ability to manipulate matter on an atomic scale. He was particularly interested in the possibilities of denser computer circuitry, and microscopes which could see things much smaller than what was possible with scanning electron microscopes. He also predicted that advances in such field would help with identifying the sequence of bases in DNA.

In 1974, Aviram and Ratner took the first step towards “molecular electronics” when they published their research that predicted the single molecules with a donor-spacer-acceptor structure would show rectifying properties when connected between two electrodes [4]. Their work showed that an organic molecule could have rectifier properties, hence could behave like a p-n junction. Aviram and Ratner used the substituent groups on aromatic system, and followed the principle of possibility to increase or decrease the pi electron density within the organic molecules, to create relatively electron-poor (p-type) or electron–rich (n-type) molecular subunits. All these compounds would withdraw electrons and make them relatively poor in pi density. In order to raise the electron affinity to make the subunits a good electron acceptor, the donor and acceptor molecular subunits in the electronic system were allowed to interact strongly with one another so that a single donor level always existed. To maintain the device

function, the donor and acceptor sites were properly insulated. Then a single molecule was put in and the whole function was accomplished by the use of a sigma-electron system between the donor and acceptor pi subunits. The molecule clearly showed rectifier properties; electron current only passed from left to right, along the system cathode to acceptor to donor to anode. In this system, whenever the applied field became large enough for the cathode levels to overlap the acceptor level, the electron transfer to the acceptor was achieved. The electrons motion was from acceptor to donor under the action of the field. The occupied ionized donor had the affinity level and holes very close to each other in energy so the electron tunneling process could take place. This whole process is also based on current passing through the rectifier molecule in three steps which mimic the equivalent-resistance net: The charged acceptor would always contain an electron in orbital B which is the charge passing from cathode to acceptor, the charge tunneling of conversation of energy to empty orbital C as acceptor to donor, and the donor to anode transfer.

In the first step, an internal tunneling of charge transfer takes place from donor level to the acceptor level. As a result, the right side contains a hole and the left an electron. After the initial steps, charge tunneling would occur in both directions between charged level and metals. The threshold voltage also plays a big role here. It is crucial to understand that the charge always flows from the highest occupied molecular orbital C on the right, which has higher energy to the acceptor π affinity orbital B level and never in the opposite direction. This non-reversible property of the internal tunneling gives the rectification characteristics to these molecules. Aviram and Ratner used the passage of electric current through a molecular system and defined as perturbation energy. They used eigenstates to find the energy in different states: from cathode to acceptor, acceptor to donor and donor to anode.

At the end, the current-voltage (*I-V*) characteristics were presented for donor ionization potential, acceptor electron affinity, and electrode work function. The *I-V* plots clearly verified the evident rectification of the single molecule: current passed preferentially to the right. The

current passage was determined by the voltage which set a threshold potential for the charge transfer to take place between the states and the respective metallic steps. The important point of this work was that the calculations verified the possibility of using a single organic molecule as a functional device.

1.3 Candidates of Molecular Electronics

In the last decade, an assortment of organic and inorganic molecules stood out as candidates for molecular electronics because of their unique chemical and electronic properties [16]. Advanced research on molecules which could form donor-acceptor system became more prominent and convenient by the advancement of micro-fabrication of metallic electrodes with nanometer scale separation. Conductance measurements on a single molecule between two terminals have been achieved by scanning probe microscopy [17-19]. Numerous scientific efforts have been documented which aimed to develop gold nanoparticles for medical applications, like cancer detection, drug delivery, and focusing of heat to locally destroy tumor cells. Recently, researchers at the University of Washington reported combining gold nanoparticles with fluorescing quantum dots, allowing for both disease detection and heat delivery in one package. Also, carbon nanotube (CNT) have been the center of attention for the last decade or so and have been found to have numerous useful applications in molecular electronics. As the systhesis of CNTs became easier, these have been used in transistors and simple logic circuits, among many other applications [20, 21]. Quantum dots are another very interesting addition in the molecular electronics community for their unique properties and wide range of applications. From disease detection to drug delivery or fluorescence imaging, quantum dots have shown immense potential in the bio-medical field. Finally, DNA (deoxyribonucleic acid) has also drawn considerable attention, a lot more than any other candidates, in the field of molecular electronics. DNA has been used as a molecular wire, since its unique characteristic of base pair stacking in double helix structure provided possible pathways for charge transport [22]. Also, DNA has unique structural motifs and excellent self

recognition and self-assembly properties because of the complementary nature of its base pairing.

1.4 Application of molecular electronics in bio-chemical sensor

This section discusses different types of conventional bio chemical sensors in use and elaborates a comparison among them. A sensor is generally a device which transduces a physical or chemical parameter into a signal (electrical, optical, change in mass, etc). Physical parameters which are commonly monitored with sensors are temperature, pressure, force, magnetic field, etc while chemical parameters of interest most often are the concentrations of chemical substances.

The applications for bio-chemical sensors are innumerable. There is a growing need of advanced and multi-functional sensors which can provide very high precision measurements for various samples. New sensors are required that enable rapid analysis at low cost, in medicine more important so appropriate treatment can be started at an early stage of disease. Sensors which are cheap and easy to use will also facilitate decentralization of chemical analysis. Another very important aspect of bio-chemical sensors is continuous monitoring of chemical parameters over a prolonged period of time. This is an area which has been subject of huge body of research. Sensors for monitoring anesthetic gases, blood gases such as oxygen and carbon dioxide, potassium and calcium levels of human body are being developed further, especially with the help of MEMS technology and biocompatible encapsulation. A brief description of different technologies used to make sensors is given here to draw a comparison among them.

1.5 DNA and Biological Sensors

1.5.1 Enzyme electrode sensor

A very commonly used sensor for biological species is the enzyme electrode sensor, where a collection of immobilized enzyme reactor is used on ion selective electrodes. There are various methods to attach enzyme on electrodes. One of them is to entrap soluble enzymes to

membranes on the electrode. Also, physical immobilization of enzymes have been done in polyacrylamide gel layers and some are chemically linked to the electrode [23]. Different kinds of ion-selective electrodes were used with enzyme electrodes although the most successful ones are the gas sensitive electrodes for gases like NH_3 and CO_2 which provides high selectivity of the gas permeable membrane. The main advantage is the effective prevention from any interference from ionic species in the analyte [23].

1.5.2 ChemFet DNA/biological sensor

ChemFet biological sensor uses the chemical parameters with ion-sensitive field effect transistor (ISFET). In a conventional MOSFET the current flows along the semiconductor surface between two contacts known as source and drain. There is a thin oxide layer on the surface and on top of that is the gate electrode made from a metal layer. When an electric potential is applied to the gate electrode, it induces the rich charge carrier layer at the semiconductor surface, commonly known as an inversion layer, which carries the current. The applied gate potential controls the current without any current passing through the gate terminal. In ISFET, the same transistor idea was used by omitting the metal gate electrode and using the underlying insulator layer as a pH sensitive membrane [23]. Since it is proven that silicon dioxide insulator in the transistor is not very stable when exposed to electrolytes, the ISFETS are usually coated with a pH sensitive silicon nitride layer for a very stable barrier. It is also possible to produce different kind of ions by depositing different electrochemically active materials on top of silicon nitride membrane which acts as a sensor. By using different sophisticated coatings, transistors can be made sensitive to various biological substances. These types of transistors are commonly known as enzyme field-effect transistors (ENFET) and their detection methods as well as sensitivities are similar to the principles of potentiometric enzyme electrodes.

The two commonly used DNA/Biological sensors do have their disadvantages. First, it is impossible to replace a damaged sensor during the measurement process. Secondly, it has

the capability to measure only one ISFET at a time. With these kinds of sensors, the measured potentials are often varied. Since it depends on the distance between the series assembled sensors and the reference electrode, slight change in distance would cause a difference in measured potential [24]. Additionally, it is reported many places that sample leakage is another source of problem. Finding these leakages is extremely difficult during the measurements because of the presence of numerous O-rings in the system sealing. If a leakage is detected, the user needs to change the o-rings by dismantling the whole system. Dismantling the whole system is also needed if the sensor is damaged and needs to be replaced. Moreover, the contact pin could destroy the back surface as well as the whole sensor during the mounting process because they are scattered in a twisted fashion all over the surface. Also, because of the black, non-transparent features of polymer material of the cell, it is very difficult to control the process of de-aeration in a particular system. All these problems are seemingly great and cried a demand for a novel approach to DNA and biological sample sensing. This is where the bio-nano technology comes to play, showing numerous modulated approaches in the form of optical and amperometric sensing.

CHAPTER 2

LITERATURE REVIEW

DNA is present everywhere in a living organism especially in the circulating body fluids of human. The unique characteristics of DNA have drawn enormous attention recently due to their potential use for disease diagnostics. Researchers have demonstrated various detection methods to positively detect specific genes. However those methods lack the capability to selectively detect the ultra-low abundance of DNA in a sample. In case of various life threatening diseases like Leukemia and HIV, it is very necessary to detect them at the earliest stages to have a better disease management. Various methods and state-of-the-art equipment used in medical field still lack the sensitivity to detect the lowest footprint of disease in human body, and the early disease detection is still an alluring fact. Generally, detection of ultra-low concentration of disease DNA (genes of interest) requires sample preparation steps and target or signal amplification steps, which restricted the path of rapid screening and detection of bacterial and viral pathogens. To achieve fast and selective disease detection, researchers have developed various lab-on-a-chip micro devices, but most of those devices are associated with various technical and DNA concentration issues. This part of the thesis will provide a comparison of the methods used and the lowest concentration of DNA detected from a biological sample. Here the most importance is given to the concentration of DNA in a sample solution, which is directly proportional to the specific detection of a disease in its early stage.

2.1. Direct concentration of circulating DNA by using a nanostructured tip

Yeo *et al.* demonstrated a novel approach to capture a specific target DNA using a nanostructured probe from a sample solution [25]. The nanostructured tip composed of single walled carbon nanotubes (SWCNT) and silicon carbide nanowires was fabricated using

fibril formation process [26, 27]. The DNA capture was done by immersing the nanostructured tip in a DNA solution, and by applying an alternating current (AC) electric field. The AC electric field produces dielectrophoretic force (DEP) which attracts the biomolecules in the close vicinity of the nanotip. The DEP force is the result of an induced polarization generating time-varying dipole moment in particles when it is exposed to an AC field. After the DNA attachment, the tip was withdrawn in a longitudinal direction, which induced a pulling force opposite to the direction of surface tension. In this process, the particle captured at the tip was dependent on the size of the particle, and only very minute particle like DNA would be successfully captured. After the initial capturing process, further tests were done to analyze the DNA using scanning electron microscope (SEM), fluorescent microscopy and X-ray analysis (EDS: Energy Dispersive X-ray Spectroscopy). For this experiment, λ-DNA was used with a concentration of 500 µg/mL with buffer (16 nM TRIS EDTA buffer, pH 8.0). Then the same experiment was followed by seven different DNA concentrations, among them the lowest was 1 pg/mL to the highest concentration of 1 µg/mL. The follow-up process using SEM, fluorescent microscopy and EDS made the experiment more cumbersome and time consuming. Also, after capturing the DNA, the controlled manipulation of the nano-tip to process the sample made it even harder to use. Since only one DNA molecule was captured at one time, followed by subsequent lengthy processes, this experiment lacks the efficiency and label-free detection capability. In this experiment, 1 pg/mL of DNA concentration was detected based on the fluorescent intensity measurement, which is much lower than the concentration of naturally occurring circulating DNA in a clinical sample (10 ng/mL). However, much lower detection limit is required for successful detection of some life threatening diseases in early stages.

2.2. Electrical characterization of DNA molecules in solution using impedance measurements

Liu *et al.* reported impedance measurements of fluids to examine the impact of the concentration of the double stranded DNA molecules [28]. The experiments showed the difference in solution capacitance and impedance values as the DNA molecule lengths and concentration were varied. Using the dipole moment of the DNA molecules as a function of their length, the mobile charges in and around the DNA were manipulated so that a dipole could be induced when an AC current was introduced in the aqueous solution. The following figures shows the correlation of the resistance change of the aqueous solution as the concentration and length of the DNA was varied.

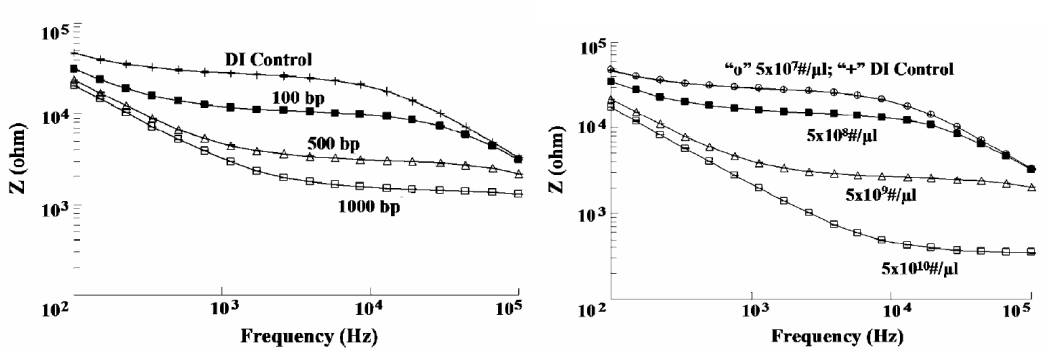

(a) (b)

Figure-2.1: Impedance versus the function of Frequency plot: (a) Showing the variation of 400 bp DNA molecule concentration, and (b) Variation of the length (number of base pairs) of the dsDNA with a concentration of each molecule was 10^9 molecules/µl [28].

The impedance of the DNA molecules was measured as a function of concentration and length. As the concentration of 400 bp double stranded DNA (dsDNA) was increased, the impedance magnitude gradually decreased, and the detection limit was set around 1 nM for the

400 bp dsDNA molecule. Similarly, the impedance magnitude decreased as the length of dsDNA molecule was increased at the concentration of 10^9 molecules/µl. Later in the experiments, three distinct DNA was used with length of 50,500, and 5000 base pairs, and similar results were found. However, an interesting trend emerged as all the curves were grouped for the different size DNA. Similar solution impedance was observed in the case of 50 and 500 bp DNA, but 5000 bp sample showed higher impedance.

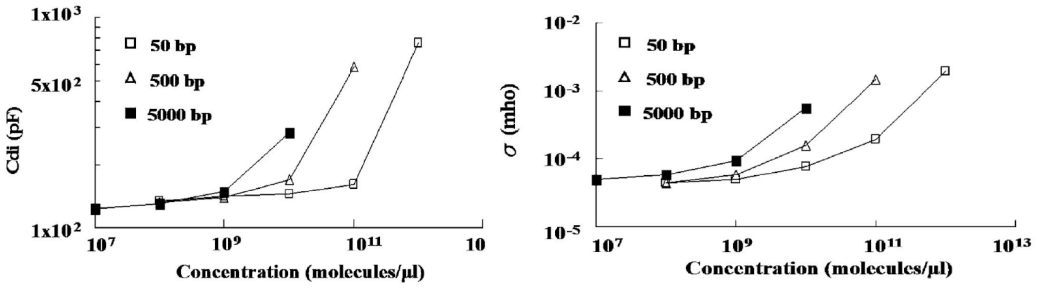

(a) (b)

Figure-2.2: (a) The solution dielectric capacitance as a function of molecule concentration, and (b) solution conductance as a function of molecule concentration[28].

After analyzing the extracted data, it was found that the electrical double layer impedance showed little variation in the perturbation energy and proved that the dominant charges are taking place in the solution. As the counterion charges move around the DNA backbone, the dielectric capacitance of the DNA was found to vary with the changes in length (bp) and concentration of DNA molecules in the sample solution. From this experiment, it is proven that the higher DNA concentration in a solution results in increased number of dipole moments, because the increased number of mobile counter-ions increases the conductivity of the solution. This observation is consistent with the studies showing DNA translocating through nanopores channels in low ionic conductivity solution because of the enhanced ionic current which is facilitated by mobile counter-ions around DNA.

2.3. Nucleic acid biosensor to detect DNA hybridization using rutin–Cu as an electrochemical indicator

Niu *et al.* performed experiments to show major intercalating role between Rutin(Cu_2R_3) and salmon sperm DNA and proved their outcome with the help of Cyclic voltammetry and Fluorescence spectroscopy[29]. Rutin is a flavanol glycoside and is of immense interest because of its anti-inflammatory, anti-tumor and anti-bacterial properties. For this electrochemical study, Cu_2R_3 and dsDNA were mixed and incubated in 0.2 mol/L B-R buffer solution and the subsequent characterization was done by cyclic voltammetric method with a potential scan from -0.2 V to 0.4 V with a scan rate of 0.1 V/sec. Then to clarify the intended binding between Cu_2R_3 and dsDNA, fluorescence spectroscopy was performed at wavelength ranging from 520nm to 690 nm with an excitation wave of 520 nm. The whole process started with the immobilization of the probe ssDNA on glassy carbon electrode (GCE) surface with 20 µL of DNA solution the concentration of 1.62×10^{-5} mol/L. The DNA hybridization event was executed with both complementary ssDNA and non-complementary ssDNA segments. The interaction of Cu_2R_3 with immobilized ssDNA was performed by immersing the GCE into 0.2 mol/L B-R buffer solution containing 1.50×10^{-6} mol/L of Cu_2R_3 at room temperature for five minutes. Then the electrochemical detection of the hybridization events was carried out by differential pulse voltammetry (DPV) method in 0.2 mol/L B-R buffer solution with a -0.4 to 0.4 V potential scan. The electrical detection outcomes were compared between bare GCE, in a solution at a concentration 1.50×10^{-6} mol/L Cu_2R_3, in a 0.2 mol/L B-R buffer solution and the other one containing 1.31×10^{-5} mol/L dsDNA solution. Figure.2.3 shows the subsequent electrical measurements.

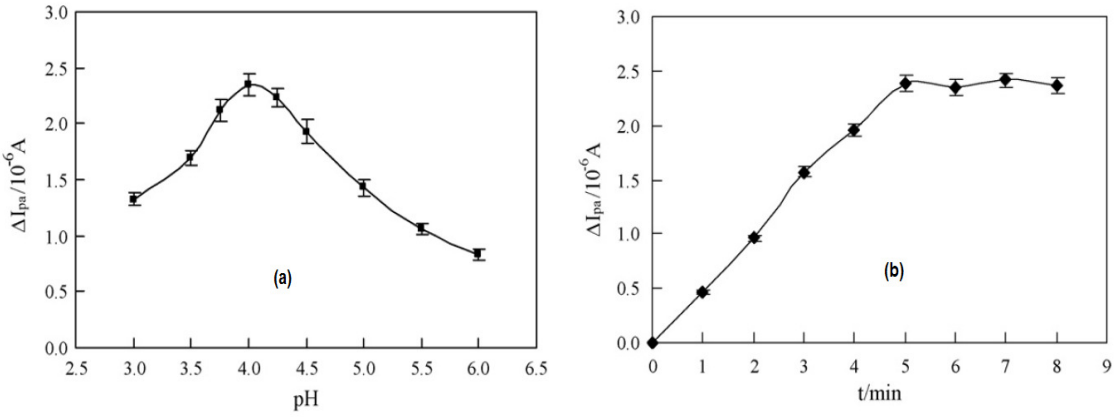

Figure-2.3: (a) Shows the relationship between ΔI_{pa} and pH. C_{Cu2R3} : 1.00×10^{-6} mol /L and CDNA: 8.75×10^{-6} mol/ L, and (b) showing the influence of the reaction time on I_{pa} of Cu_2R_3 before and after the addition of DNA. C_{Cu2R3}: 1.00×10^{-6} mol/ L and C_{DNA}: 8.75×10^{-6} mol /L [29].

The electrical detection results showed that anodic peak current of Cu_2R_3 for bare GCE in B-R buffer is 0.047 V whereas a decrease in peak current and peak potential was shifted by about 15 mV for the dsDNA buffer solution. Different experimental conditions were used later to optimize the pH value and reaction time of the Cu_2R_3 and DNA interaction. Figure.2.3 (a) shows the change in peak current with varying pH and change in reaction time. The peak current change is directly proportional to the pH of the buffer solution and the maximum occurs at a pH level of 4.0. Figure-3(b) shows the constant peak current after the incubation for 5 minutes. Further study shows that the anodic peak current of $Cu_2R_{3\ was}$ directly proportional to the square roots of the potential scan ranges from 0.02 V/sec to 0.22 V/sec, indicating a diffusion controlled electrochemical process. The whole process was then repeated again with three different probe DNA concentrations of 1.62×10^{-6} mol/L, 1.62×10^{-5} mol/L, and 1.62×10^{-4} mol/L, and hybridized with complementary target DNA with a concentration of 8.10×10^{-7} M. To obtain the subsequent intercalation of Cu_2R_3, three different probe DNA concentrations of 1.62×10^{-6} mol/L, 1.62×10^{-5} mol/L, and 1.62×10^{-4}mol/L were used and the recorded peak currents were 3.4×10^{-7} A, 5.2×10^{-7} A, and 3.9×10^{-7} A, respectively. The change in peak current value showed the sensitivity of this electrochemical biosensor depends on the concentration of DNA in the

solution. The difference of oxidation peak current value was linear with the concentration of target ssDNA ranging from 1.62×10^{-8} mol/L to 8.10×10^{-7} mol/L. The increase in differential pulse voltammetry (DPV) peak current also proved that the probe DNA specifically recognize the complementary target DNA sequence and a linear relationship of current vs DNA concentration was also established.

2. 4. Conjugated-Polymer/DNA Interpolyelectrolyte Complexes for Accurate DNA Concentration Determination

Hong *et al.* demonstrated a very unique approach to quantify the concentration of DNA using a polymer called PFPB [30]. A cationic water soluble poly ((9,9-bis(6′-N,N,N,-trimethylammoniumbromide) hexyl)fluorene-co-alt-1,4-phenylene) was used which changes color depending on the DNA concentration. In dilute condition, this polymer has negligible aggregation and emits in the blue region of the electromagnetic spectrum (390-500 nm). When it is mixed with certain DNA, which increases the aggregation, interchain contacts and promotes better coupling between electronic and optical contacts, it starts emitting in the green region. This sort of behavior is due to the increased energy transfer mechanism like energy hopping compared to the energy transfer in the backbone. The addition of the negatively charged polyelectrolyte like DNA produces cooperative electrostatic interactions, which induces complex formation as well as raising the local PFPB concentration.

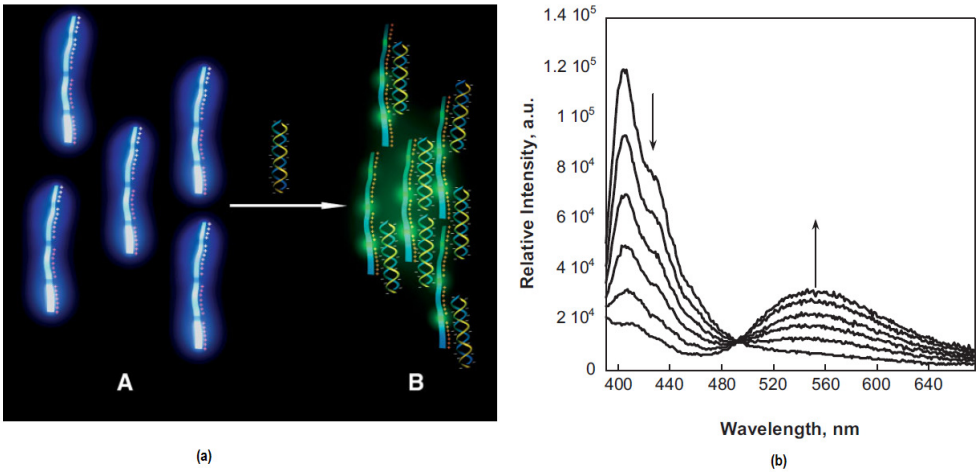

Figure-2.4: (a) Shows the PFPB color changing from blue to green as DNA is added satisfying the Förster resonance energy transfer conditions, and (b) showing the PL spectra of $PFPB_7$ (1.0×10^{-6} M) with 3.6 µL additions of 5.1×10^{-6} M of 20 bp dsDNA (emission maximum k_{ex} = 380 nm) [30].

To quantify the shifting of emission color with the addition of DNA, a parameter σ was defined to normalize the data across different instruments and optical conditions and followed by the equation:

$$\delta = \frac{G_n - G_0\left(\frac{B_n}{B_0}\right)}{N} \qquad \text{.....(1)}$$

where G_0 is the integrated green fluorescence (500-700 nm), G_n is the integrated green fluorescence at the *n*th addition of DNA, B_0 is the integrated blue fluorescence (390–480 nm) in the absence of DNA; B_n is the integrated blue fluorescence at the *n*th addition of DNA; and N is the normalization factor, obtained by the emission (390–480 nm) of a 1.0×10^{-6} M $PFPB_7$. A series of experiments were done to provide a comparison of the optical responses of different polymers after the addition of DNA, where δ was plotted against dsDNA. From the plots, a remarkable linear relationship was observed between δ and dsDNA in a certain concentration range and for all structural compositions.

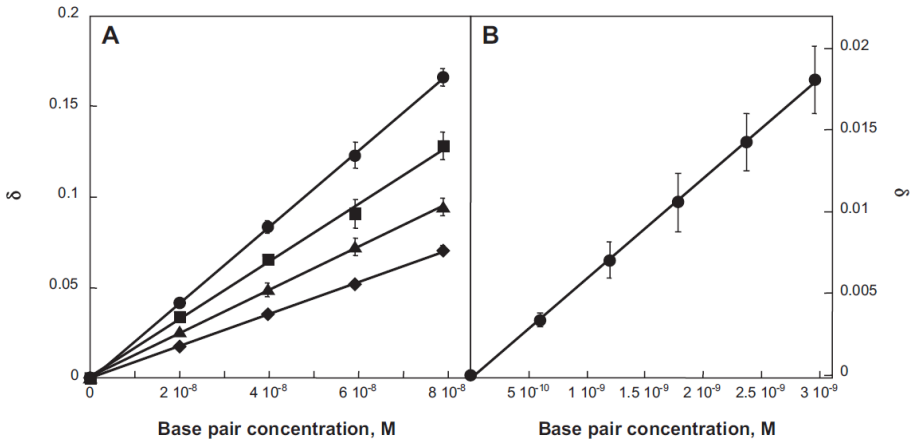

Figure-2.5: A) δ for $PFPB_1$ (♦), $PFPB_{2.5}$ (▲), $PFPB_5$ (■), and $PFPB_7$ (●) as a function of bp concentration for 30 bp dsDNA. B) δ for $PFPB_7$ (●) as a function of bp concentration for 30 bp dsDNA in the concentration range of 6.0×10^{-10} to 3.0×10^{-9} M [30].

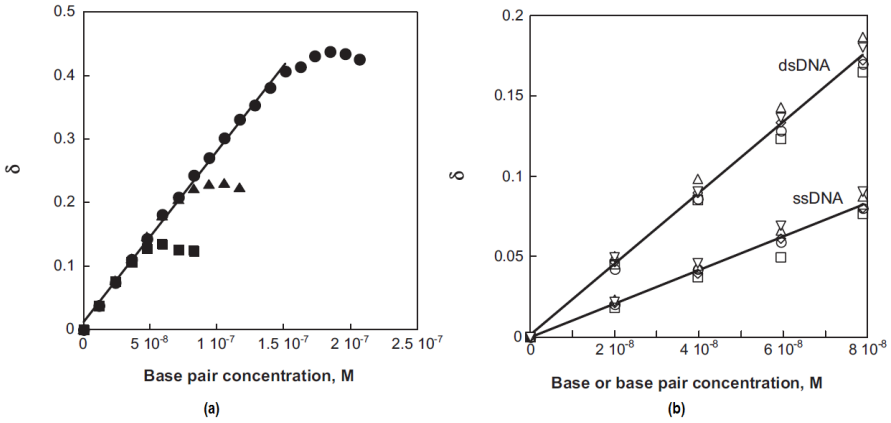

Figure-2.6: (a) shows δ as a function of bp concentration of 30 bp dsDNA for $PFPB_7$ at [RU] = 2.5×10^{-7} M (■), 5.0×10^{-7} M (▲), and 1.0×10^{-6} M (●), and (b) showing σ as a function of bases f or ssDNA and base pairs for dsDNA :(ss20 (Δ); ss30 (o);ss50 (◊); ss75 (▼); and ss100 (□)) and dsDNA (ds20 (Δ); ds30 (○);ds50 (◊); ds75 (▼); and ds100 (□)) .

Figure.2.6 (a) illustrates two significant features; the response of δ to 30 bp dsDNA at three different $PFPB_7$ concentrations where the similar slopes in the low concentration zone shows the response is independent of $PFPB_7$ assay, and the δ versus dsDNA plot levels off at the high concentration zone. This means that once the RU/bp ratio is reached at that limit, an increase in response is no longer possible. The experiment was pushed further to see the possible changes in light emission with the changes in bases and base pairs (chain length) in ssDNA and dsDNA. Taking a range from 20 to 100 bases and base pairs, further experiments

was conducted and the results were plotted as in figure 6(b). The plot shows δ as a function of ssDNA and dsDNA at different lengths of DNA using $PFPB_7$. As for the scheme of changing color dependence of DNA base and base pairs (DNA strand lenght), shades of green were found to depict different detection sensitivities. This DNA detection scheme is not as sensitive as some of the industry standard procedures, but it shows excellent accuracy, repeatability and could be done efficiently in short period of time.

2.5. Sequence-Specific Detection of Femtomolar DNA via a Chronocoulometric DNA Sensor (CDS)

Zhang *et al.* reported a novel nanoparticle based electrochemical scheme for DNA detection [31]. A "sandwich" strategy was employed to immobilize probe DNA on gold electrodes and reporter probe DNA labeled with gold nanoparticle were then introduced to flank the target DNA sequence. To detect the presence of specific DNA, electrochemical signals were generated by chronocoulometric method using $[Ru(NH_3)_6]^{3+}$. A single gold nanoparticle attached with hundreds of reporter DNA strands significantly amplified the signal and helped in the detection of DNA. If the target DNA is absent, there is no formation of the sandwich complex hence the surface confined capture probe DNA was left unhybridized.

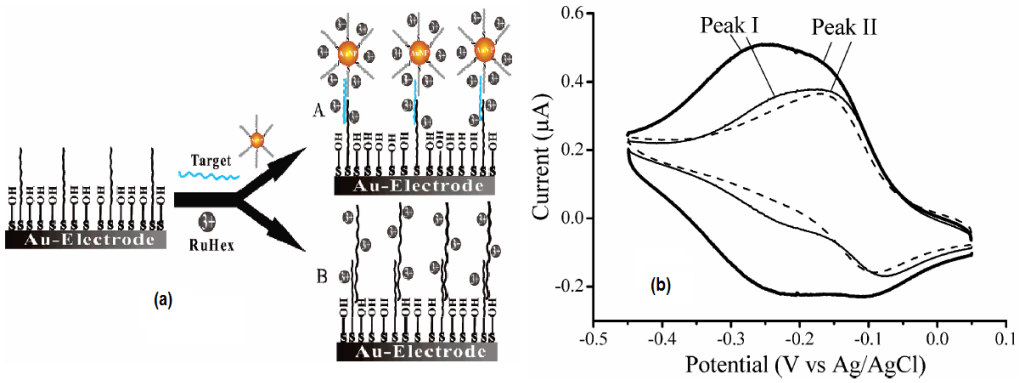

Figure-2.7: (a) Graphically showing the whole capture and target probe DNA scheme with gold nanoparticle for signal amplification, and (b) showing Cyclic voltammograms of gold electrodes modified with capture probe DNA. Dashed line showing 50 μM RuHex before hybridization and solid line showing after hybridization with 1 µM target in the absence of AuNP amplification. Thick line showing 10 pM target in the presence of AuNP amplification. Scan rate = 50 mV/s [31].

The RuHex was used in this experiment as a signaling molecule in the chronocoulometric DNA sensor (CDS). Signal transduction showed two pairs of peak as in figure 7 (b). Peak I is the result of redox reaction of RuHex electrostatically attached to the phosphate backbone of DNA. Peak II is due to the RuHex diffused to the mercaptohexanol (MCH) part in the mixed self assembled monolayer of DNA/MCH. Then to quantify the DNA hybridization efficiency with respect to the sensitive function of surface density of immobilized DNA capture probes, a series of DNA SAMs were prepared with different surface density, by varying probe concentration, self-assembly time, and ionic strength in the immobilization buffer. The results clearly showed that control of DNA assembly and perfect complementary/mismatch base pairs were the key ingredients for DNA sensitivity, and low-density DNA monolayers provided the path for high-sensitivity DNA detection.

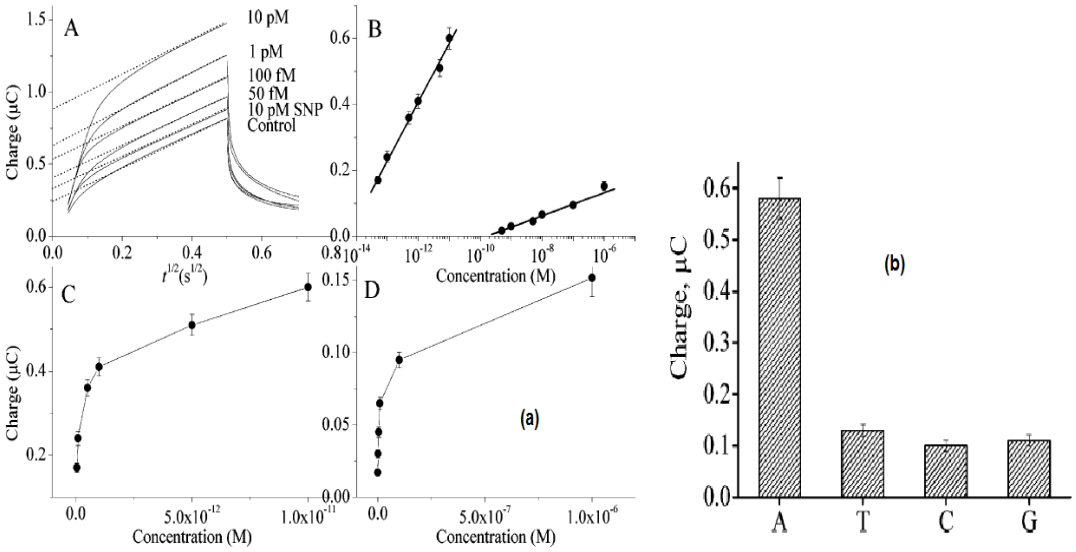

Figure-2.8: (a) Shows the Chronocoulometry curves for electrodes with capture probe **1** hybridized with target DNA at a series of concentrations (50 fM, 100 fM, 1 pM, and 10 pM), and with 10 pM single-nucleotide mismatched (SNP) DNA. (B) Logarithmic plot of signal versus target DNA concentration, where the definition of signal is the same as that in figure (C) and (D) are the original plots (without logarithmic conversion) for detection in the presence and in the absence of AuNP amplification, respectively. Figure (b) shows the comparison of signal intensity for gold electrodes hybridized with a series of targets at a concentration 10 pM: the perfectly matched DNA (A) and single-nucleotide mismatched DNA (T, C, G) [31].

Series of tests with different concentration of DNA proved that the redox changes of RuHex increased only after hybridization with complementary DNA, and mismatch pairs did not show any notable increase. The signal intensity was found logarithmically related to the target concentration in the range of 10 pM. Femtomolar range was also tested without any significant results. In the mismatched DNA tests, it could be easily recognized as showed in figure 8 (a), and the signal strength was found to be only 15% of the complementary DNA. Overall in these experiments, the absolute detection limit of the target DNA as reported was 0.5 nM, however, there is no information of DNA strand length. DNA strand length (number of base pairs) is also a key point to set a certain detection limit. Longer DNA strands will provide a lower detection limit

as compared to shorter strands in the same DNA concentration range, which will eventually give erroneous result as compared to different DNA strand lengths.

CHAPTER 3

ELECTRICAL MEASUREMENT OF DNA

One of the many goals of molecular electronics is the measurement and control of the electronics properties of DNA. The electrical conductivity measurement of DNA is of immense interest not only for their unique self recognition properties but also for their application in molecular electronics. However, electrical conductivity measurement of DNA is extremely difficult, and it needs extreme caution and highly optimized techniques to do it correctly. In this chapter, different techniques will be discussed that were used to study the electronic transport properties of DNA. These will include different methods of DNA conductivity measurements and their fabrication techniques.

3.1 Techniques for Measuring the Electrical Conductivity of DNA

The electrical conductivity measurement of DNA has been made possible by the advancement of MEMS and nanotechnology. Photolithography and electron-beam lithography have been widely used to fabricate nanoelectrodes to connect DNA into an electrical circuit. Different techniques of breaking a junction to create a nano-sclae gap have been published by many researchers in the last decade [2, 5, 7, 32-35]. However, reproducibility is always a challenge when attaching DNA to silicon surface and between two metal contacts in such a small scale. Moreover, electrical properties of DNA also depend on experimental conditions and chemicals used and also are very sensitive to ambient temperature. In this section, different methods will be introduced for nanogap trapping of DNA and its fabrication and break junction trapping of DNA and its fabrication.

3.1.1 Break Junction Method

The ‘‘Break Junction’’ technique was first devised in 1985 by Moreland and his group at National Bureau of Standards [36]. Generally, break junction is the discontinuity or a nanoscale gap in a seemingly continuous structure. The most common visualization of a break junction is a gap formed in a thin metal strip by various methods as described in following sub-sections. The nanoscale gap in the metal strip is the area of interest where the molecule is placed to make electrical contacts. It is by far the simplest way to study charge conduction through the molecules. Based on the famous description of electronic transport through a single molecule by Aviram and Ratner [4], electronic transport through a single molecule have been reported by many researchers [37]. When connected between superconducting nodes, atoms form Josephson junction which has the ability to conduct a super-current. The super current’s amplitude is set by the number of conducting atomic orbitals, often called channels, and their transmission coefficient. With standard e-beam lithography, electrode pairs with spacing below 20 nm are difficult to define reproducibly. Therefore, several alternative methods, including electromigration method [38] or electro-deposition [39], have been done successfully for special applications.

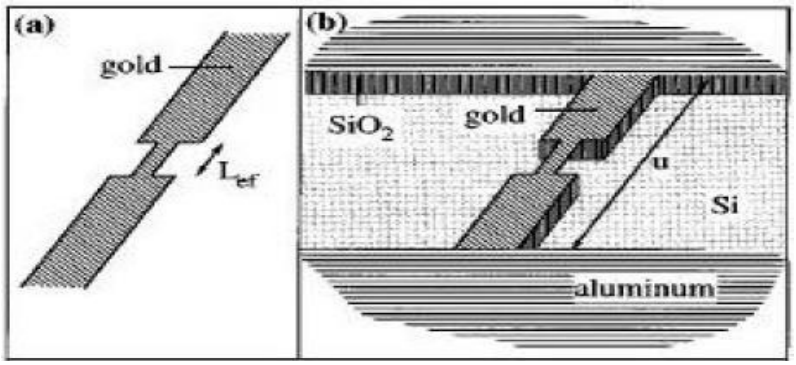

Figure-3.1: a) Electron beam lithography defined wire pattern with L_{eff} of 259 nm.(b) Structure with micro-scale contact pads [40].

There are mainly two ways to create a break junction from an already fabricated electrode, mechanically controlled break junction and electromigration break junction.

Mechanically Controlled break junction is basically a process where a narrow bridge of metal is suspended above a flexible substrate. By bending the substrate, the metal bridge can be broken, and the distance between the ends can be controllably adjusted, with increments of much less than a pico meter.

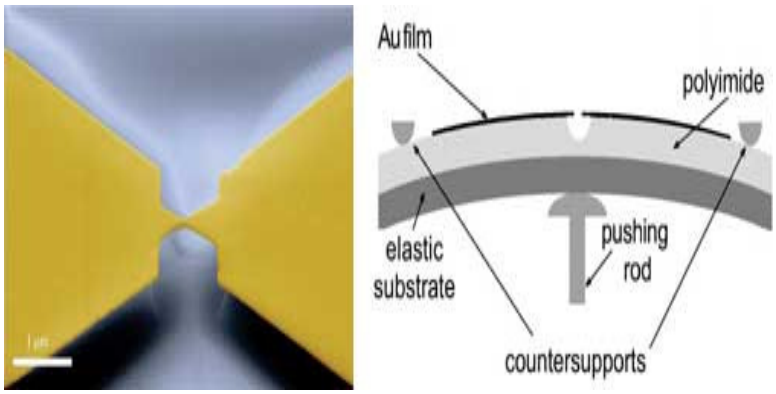

Figure – 3.2: Top view and schematic illustration of mechanically controlled break junction [41]

To create break junction using electromigration, an external electric field applied to a circuit causes large current density in the wires that connect the components. The electrons in a metal move under the influence of the large current density and if there is a charged defect in the metal, the momentum transfers from the conduction electrons to such a defect. As the momentum exchange becomes larger and larger, a force is built up causing the mass movement of the atoms away from the defect causing breakdown of the metal at that point. In break junction, the break usually occurs in the constricted part of the metal in a controllable and self-limiting fashion. Normally, the breaking process consistently produces two metallic electrodes at typical separations. These electrodes have been widely adapted for electron-transport studies of molecules and nanocrystals. Figure.3.3 illustrates the *IV* characteristics of a break junction both before and after the nanogap creation.

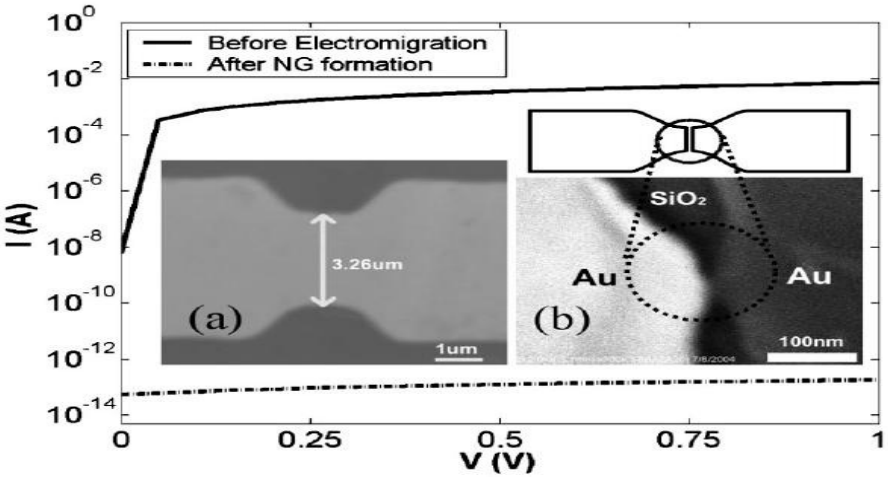

Figure- 3.3: *IV* characteristics of the break junction show a significant drop of current from 3-5 mA to 0.3 nA after the formation of nanogap. (a) Break junction before elctromigration and (b) after electromigration [10].

3.2 Different techniques of break junction fabrication

There are several techniques to fabricate break junctions. Almost all of them follow the conventional process of thin film deposition, lithography and etching on oxidized silicon wafers. The distinguishing factors are the way it's done and the process flow. The following are few techniques to fabricate break junctions.

3.2.1 Fabrication Method – 1: Microfabricated Break Junctions

Zhou *et al.* used microfabrication techniques to fabricate mechanically controllable break junction on a silicon substrate [40]. Electron beam lithography (EBL) was used to put a pattern in an e-beam sensitive photoresist known as PMMA (Poly methyl methacrylate) on an oxidized Si wafer. Thin metal layers of Ti/Au (100 Å/800 Å) were deposited using e-beam evaporation as shown in Figure.3.2. The second metal layer of Al was deposited using photolithography on the oxide with the exception of Au features.

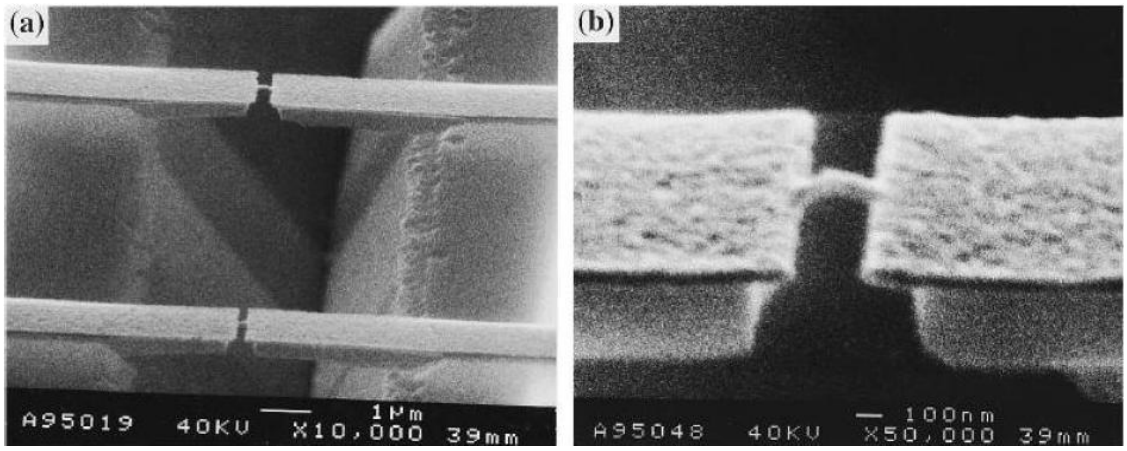

Figure-3.4: (a) Break junction suspended above a triangular trench in the Si substrate after anisotropic etching process.(b) SEM images of a Au wire connecting the cantilevers [40].

Using Au and Al films as hard mask to protect the area of interest, the SiO_2 and Si layers were etched by CF_4/O_2 plasma. Wet processing was used to remove the exposed Si area followed by the removal of Al. A triangular pit was formed in silicon by aligning the Au structures in <110> direction, where the edges were surrounded with SiO_2 and the <111> surfaces. The Au metal line eventually became two free standing cantilevers when an etchant was used to perform a rapid undercutting at the convex corners. The final device resulted in two small cantilever beam with dimensions of 4 μm by 2.5 μm connected by a narrow 100 nm wide wire. Then the break junction was created by mounting the device on two 20 μm apart counter support and applying a controlled force on the backside via a piezo element using a coarse adjustment screw. The stretching of the silicon beam created fracture on the Au wire, which was the final break junction while the silicon substrate stayed intact.

3.2.2 Fabrication Method – 2: Shadow Evaporation Break Junction.

Park *et al.* reported another method to fabricate 20 nm Au wires by EBL and shadow evaporation [38]. A 200 nm long suspended resist bridge was created 400 nm above a SiO_2 substrate with the help EBL on a PMMA and co-polymer (PMMA-MAA) bilayers. They evaporated Cr/Au (35 Å/ 100 Å) to make metallic nanowires at an angle of ±15° with respect to

the normal of the substrate. Two individual electrodes were generated by similar angle evaporation steps overlapped to form a metallic junction.

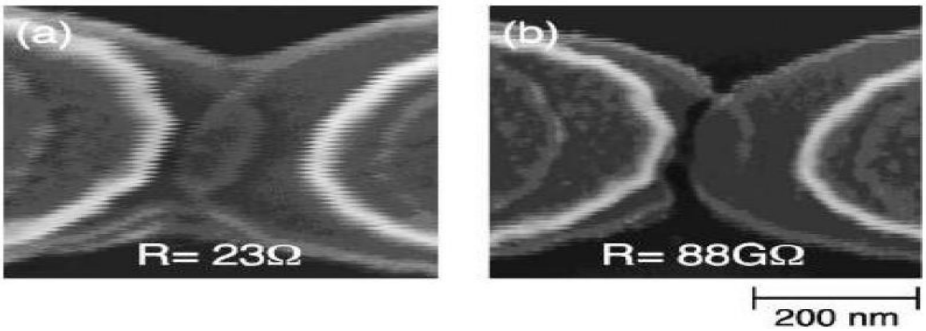

Figure-3.5: FESEM images showing Au nanowires (a) before and (b) after the breaking. The diffused white lines have separation of approximately 100 Å [38].

In the final step, another Cr/Au (35 Å/ 800 Å) layer was deposited straight down through the resist bridge to connect the nanowires and Au bonding pads (defined by optical lithography). The nanometer gaps were formed by breaking the nanowires with the passage of current. A four probe configuration was utilized to characterize the breaking process by monitoring the voltage drop across a nanowire. The driven current also increased with the increase in applied voltage, becasue they are directly proportional to one another. At the beginning of electromigration, the conductance began to drop. Additional increases in current resulted in the conductance dropping rapidly to almost zero, indicating the breaking of the nanowire. The whole process was replicated for below 20 nm thick Au nanowires. An example SEM image of a broken wire is shown in Figure 13 (b). The failure or break in the nanowires mostly occurred near the region where two angle-evaporated electrodes overlapped, since the thinner metal films had high resistance. The usual resistances of broken lines were around 10 GΩ and the range varied in some devices having lower range of few hundred kΩ to higher range of 200 GΩ. Current leakages through the SiO_2 substrate made the resistance measurement impossible for resistances larger than 200 GΩ.

3.2.3 Fabrication Method -3: EBD, nanoparticles and electrodeposition Break Junction.

In this fabrication process of break junction by EBD, a Si wafer was used and the insulating layers were made by 1 μm thick thermally grown SiO_2 and 60 nm thick ultra low-stress Si_3N_4 film made by low pressure chemical vapor deposition (LPCVD) [42, 43].

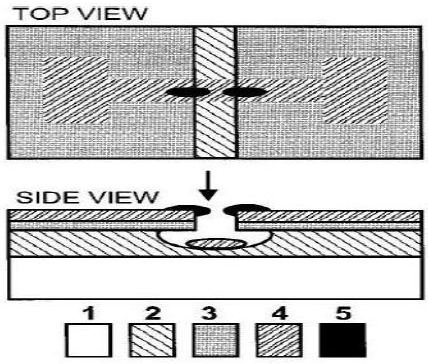

Figure-3.6: Schematic view showing (1) Si wafer, (2) SiO_2 film, (3) Si_3N_4 film, (4) AuPd film with contact pads, and (5) E-beam deposited carbon electrodes with ~5 nm gap. Arrow shows the orientation of the e-beam[42].

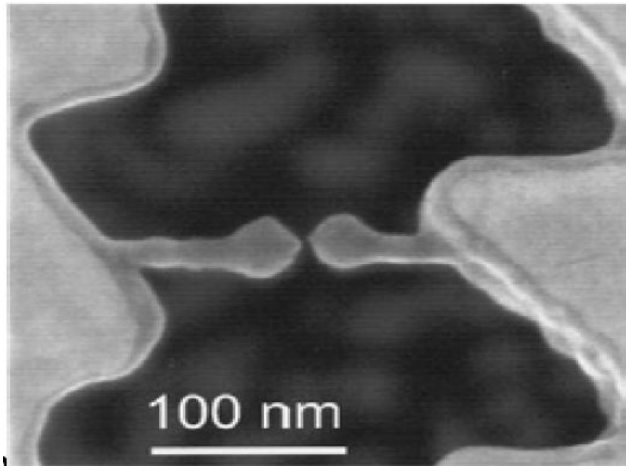

Figure- 3.7: Two free-standing carbon nanowires grown towards each other using EBD [42].

A long slit in the Si_3N_4 film was etched using RIE, and the hard mask was made by spin coating PMMA and patterning with EBL. The slit was approximately 100–150 nm wide and a few mm long. The underetching of the core SiO_2 layer was done with HF acid that provided the two free-standing Si_3N_4 overhanging structures as shown in Figure 14. A mechanical shadow mask was used afterwards to sputter an Au or AuPd strip of 10–20 nm in thickness and about 20 mm in width across the slit. Anisotropic etching in KOH was used to make the mechanical shadow mask in Si wafer. Free-standing horizontal carbon nanowires were placed by electron beam on the Au film near the permimeter of the membrane. Initially the deposition took place on the Au film, however, as soon as the beam left the membrane, a free-standing carbon needle started to grow vertical to the membrane and above the slit. The definite pattern of the growing carbon rod was controlled by periodically scanning the beam at high speed across the slit, and then gradually slowing down until the carbon wire could follow the beam. The approximate width of e-beam deposited needles was between 5 and 20 nm (Figure 15) and could be reduced down to about 3 nm by slow oxygen plasma etching process. The SEM was zoomed in on the nanowires near the gap, i.e., (the tips of both carbon needles) in order to reduce the gap between the electrodes. As the nanorods grew directionally towards each other, gap between them was eventually decreased. When the distance between their tips reached desired value, the SEM was switched off. The minimum gap size achieved by this method was less than 3 nm.

3.2.4 Fabrication Method-4: Lift – off Technique Break Junction:

This method is perhaps the most popular one. The process flow is as below:

1. Starts with wafer processing (Si wafer).

2. Oxidation: Insulating dielectric layers are a key element in break junction fabrication which provide isolation between conductive layers on the surface of the wafer. Dielectric mostly silicon dioxide, is deposited.

3. Spin coat photo resist (PR).

4. Pattern the photo resist (Mask -1) using a mask aligner. This would make a 3-5 um wide gap. Expose to UV light.

5. Deposit Ti/Au using e-beam evaporation. Ti is used because Au does have very low affinity to SiO_2.

6. Perform lift-off technique. Lift-off is a simple, easy method for patterning films that are deposited. A pattern is defined on a substrate using photoresist. A film, usually metallic, is blanket-deposited all over the substrate, covering the photoresist and areas in which the photoresist has been cleared. During the actual lifting-off, the photoresist under the film is removed with solvent, taking the film with it, and leaving only the film which was deposited directly on the substrate.

7. Clean the Chip.

8. Spin coat PR again.

9. Align and Expose second mask (Positive mask). This is for the contact pads on either side of the break junction.

The complete process flow is shown in figure 16 and 17.

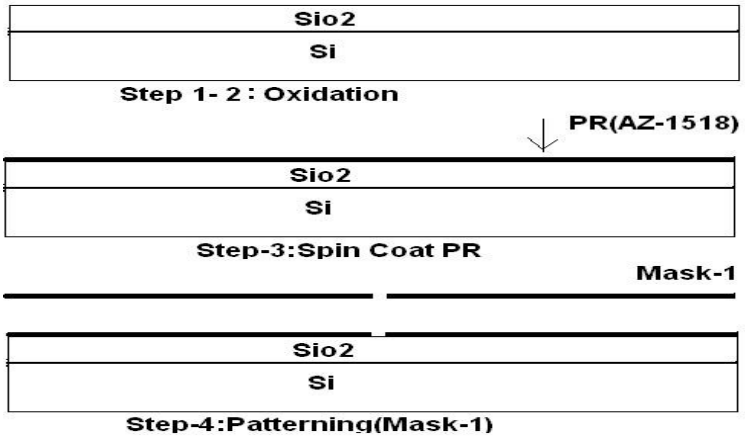

Figure- 3.8: Process flow for the steps 1 - 4.

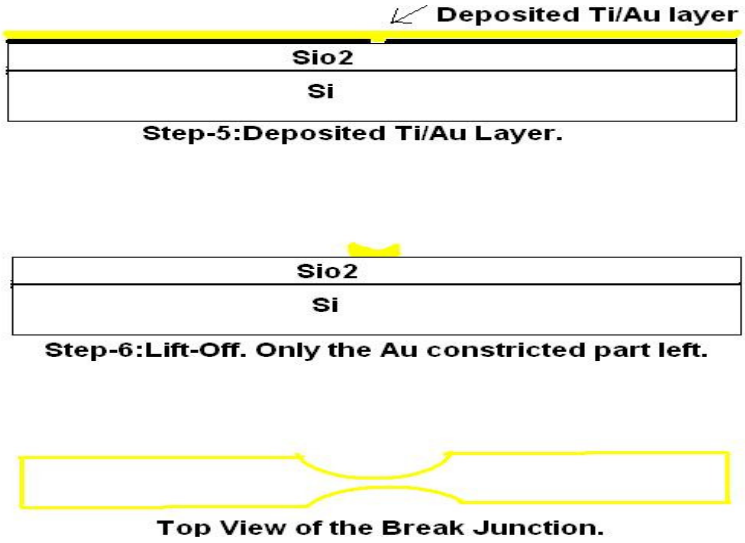

Figure- 3.9: Step 5 – 9.Some of the steps are skipped.

3.3 Nanogap Electrode method

Fabrication of controlled nano-gap electrodes is another efficient method of trapping DNA. This method also follows the same procedure of integrating single or double strand DNA into a circuit using metal electrodes to perform conductivity measurements. The separation between the electrodes must be small in accordance with the length of DNA molecules used. Since such distances eliminate the chances of direct tunneling currents, there exists no other parallel conduction path other than the conduction through the DNA. Thus, these types of setup ensure the measurement of real electrical current through the DNA. However, DNA conductivity also depends on the measurement methods, ambient environment of the samples, humidity and temperature. In particular, the gap between the electrodes is the most crucial factor in the conductivity measurement. Metal electrodes are usually fabricated by photolithography on silicon wafer with an insulating silicon dioxide or silicon nitride layer. For nano-scale gap, advanced photolithography techniques such as EBL or focused ion beam (FIB) etching is generally used. For bulk processing in the semiconductor industry, photolithography using very short wavelength (currently 193 nm) laser is the predominant fabrication method generally used.

IBM and other companies use high-index immersion lithography techniques to produce features less than 32 nm. For research purpose, Morpurgo *et al.* fabricated metal electrodes with less than 1 nm separation using conventional photolithography and electrochemical methods [39].

EBL is usually done by coating a silicon wafer with electron beam sensitive chemical such as PMMA (poly methyl methacrylate) or HSQ (Hydrogen SilsesQuioxane) in a spin coater and then writing the pattern with electron beam. The required pattern can be drawn using any compatible CAD software and then uploading in the e-beam machine. Even though it sounds very straight forward, getting the right pattern is a hard task since it involves lot of characterization process. EBL is one way to overcome the diffraction limit of light and make features in the nanometer regime without using a conventional mask. FIB is another method of creating nano-scale gaps in metal electrodes. FIB could be used to rapidly etch away metal on silicon wafer, thus creating nanometer separation. FIB etching is onestep micro-machining technique, in which no photolithography is required. Furthermore, a computer program can control the entire etching process automatically, and could enable spatially selective, mask less, patterning and processing of materials at extremely high levels of resolution. Nanogap junctions could be obtained in a matter of few minutes from metal patterns such as lines created by photolithography. FIB is also very useful to create nanopores on silicon and PDMS block. FIB process with different milling conditions is applied to create single nanopores or circular nanopore arrays with a different number of opened pores on different kind of substrates. This is a low cost process, and offers an economically viable alternative for the fabrication of nanopore devices with controlled dimensions for a range of applications in nanofluidics, molecular separations and biosensing. The nanogap junctions were also created in Au metal layer on top of silicon nitride film. Similarly, nanopores were created in 30 nm thick silicon nitride film sandwiched between 60nm of Ti/Au layers. Following are some of the FESEM images of FIB created nanogap junctions and nanopores.

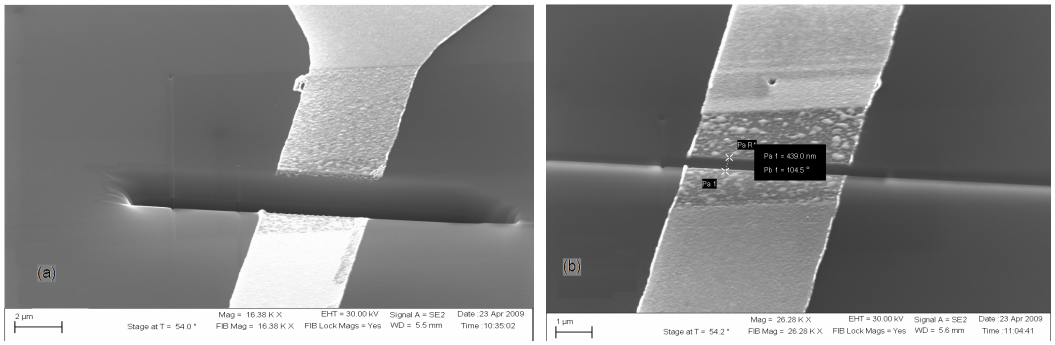

Figure-3.10: (a) Nanogap Au junction created by FIB milling on silicon dioxide surface. (b)FIB created nanogap of 430 nm.

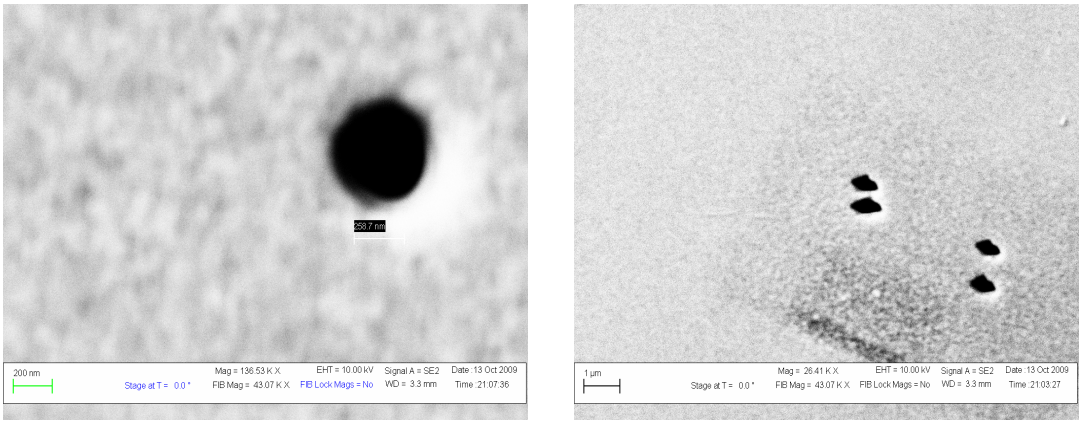

Figure-3.11: FIB milled nanopore and nanopore arrays.

3.4 Electrical conductivity of DNA

Electrical conduction through DNA and its charge transport has been shown to be modulated by intervening sequence [44] and such effects of sequence or hybridization have been investigated before [10]. A lot of work has been done with various DNA strands and biological agents using break junction, to characterize the electrical properties [2-10, 12]. It has been established that a number of factors and conditions contribute to the behavior of DNA conductivity; [6, 45] the number of bp, the sequence and length of DNA [46], change in rise (the

distance between bases) and twist (angle between consecutive bases), influence of water and counterions, humidity, contact chemistry, surface smoothness, electronic contamination, ambient conditions, temperature and buffer solution components.

In 1962, an article, "Semiconductivity of Organic Substances" by Eley and Spivey showed that the DNA structure was ideal for electron/hole transfer, and charge conductance through DNA molecule can take place in a single dimensional pathway constituted by the overlapping π-orbital in neighboring base pairs [1].

$$\sigma = \sigma_o \exp\left(-\frac{\Delta E}{2k_B T}\right) \tag{2}$$

At temperature of 400 K, conductivities were found in the order of 10^{-12} $(\Omega\ \text{cm})^{-1}$ and energy gaps (ΔE) of about 2.42±0.05 eV.

Researchers from Delft University of Technology reported the conductivity of 30 bp 10.4 nm long poly(G)-poly(C) ds-DNA electrostatically trapped between two 8 nm spaced metal electrodes [46]. They concluded that the DNA strand behaved like large band gap semiconductor with a voltage gap at low biases as shown in Figure 3.12.

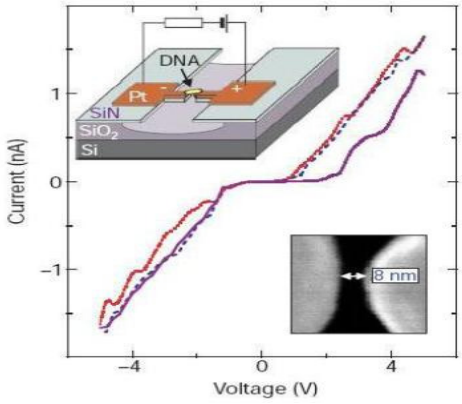

Figure-3.12: The *I-V* curves measured at room temperature of the DNA molecule trapped between two metal electrodes [46].

Lee *et al.* reported how the oxygen adsorption affected the conductance of DNA [47]. They fabricated Ti/Au electrodes of gap ranging from 100 to 200nm using same poly sequence as Yoo *et al.*[2]. The *I-V* data was measured at room temperature at humidity of 35% and then compared with the data taken in vacuum and in a mixture of oxygen-nitrogen (1:4). The resistance increased from about 0.8 GΩ to 7 GΩ to 100 GΩ, for poly (dG)-poly (dC) DNA at 1 V, for the room ambient, vacuum and controlled oxygen nitrogen mixture, respectively. The increase in resistance was caused by the modulated oxygen content of the measured conditions as trapped oxygen doped the DNA with holes. Further experiments revealed that the change in oxygen content increased the DNA conductance of poly(dG)-poly(dC) DNA by more than 100 times when exposed to pure oxygen instead of air. They also reported the behavior of poly (dG)-poly (dC) DNA as p-type conductor and poly (dA)-poly (dT) DNA as an n-type conductor.

Hwang *et al.* also reported using nanogap and micron scale Au electrodes to measure *I-V* of 60 bp poly (dG)-poly (dC) DNA [8]. Nitrogen gas was used to dry out the DNA once deposited between the electrodes. In 30 μm apart electrodes, almost linear *I-V* characteristics were observed; whereas clear staircases were observed in the dI/dV plots for 100 nm gap electrodes. For the smaller gap (compared to micron scale gap) trapped DNA, the average voltage interval was 2.5 V. Further experiment were done by taking *I-V* measurements in vacuum to exclude the effect of moisture and they reported no change in the ionic conduction or effect of O_2 doping [8]. Same results were found when they repeated the experiments by using thiol-modified DNA in Au electrodes. The DNA molecules attached to Au nanoparticles were chemically anchored between Au nanoelectrodes, and participated in making an electrical conduction channel [48].

In 2000, Cai *et al.* also performed direct electrical measurement of DNA with conductive atomic force microscopy (c-AFM) at room temperature [34]. Two different DNA (poly (dA).poly(dT), poly(dG).poly(dC)) were used separately on cleaved mica surface. Poly

(dA).poly(dT) DNA forms a cross-linked bonding with mica surface, wherees poly(dG).poly(dC) forms a uniform reticulated structure. Afterwards, a gold electrode was fabricated to make contact with DNA network in one end while a moving conductive AFM tip was used to make contact with DNA at different positions. To characterize the electrical conductivity, noise current were specifically observed when the AFM tip touched the bare mica surface without the DNA. Linear ohmic and p-type rectifying behavior were both observed for poly(dG).poly(dC) when the AFM tip was approximately 100 nm away from the gold electrode. For poly (dA).poly (dT) DNA, only linear ohmic behavior with much higher resistance were observed. This led to the conclusion that the ions (H^+ , Na^+) in the buffer solutions might have affected the π – stacking electronic structure of DNA, which eventually affected the charge transport.

Xu *et al.* demonstrated an elegant method to study the conductivity of DNA in aqueous solution using mechanical break junction with STM where the thermal motion and native conformation of the DNA stays well preserved [9]. Two series of 8, 10, and 12 bp of DNA sequences were used to separately form double helix structures with $CH_2CH_2CH_2$-SH group at both ends. Statistical analysis was done by creating conductance histogram from the data taken from over 500 individual measurements. In the histogram data, 8-bp dsDNA showed defined peaks near integer multiples of $1.3x10^{-3}G_0$ while the control experiment without DNA in the solution showed no such conductance. Two different methods were used to obtain the *IV* curves of a single DNA duplex. In the first method, several conductance histograms were constructed to derive the main peak at different bias voltages while the second method measured the *IV* curves with sweeping voltage by stopping the tip at the last conductance point. The *IV* curves from both the methods, which correlated the conductivity of DNA duplex in the gap between the tip and gold surface, showed similar linear ohmic behavior from -0.5 to 0.5 V. This experiment was very significant because the DNA molecules kept their native structure intact and integrated with the electrodes by Au-S chemical bonds.

Kasumov *et al.* reported a unique experiment claiming the superconductivity of DNA in 2001 [35]. Individual strands of Re/C fibers of approximately 40 nm tall were created by sputtering 2 nm thick carbon on a 2 nm rhenium layer on mica substrate to serve as superconducting electrodes with a temperature transition at 1 K. Two electrodes were then created on Re/C film by focused laser beam and 16 μm long DNA molecules were attached in the gap by flowing in DNA solution. Around 100 – 200 DNA molecules were introduced to bridge the gap between the two Re/C bi-layer which decreased the overall resistance from 1 GΩ to few KΩ. Further analysis revealed an average figure of 300 KΩ of resistance per DNA molecule. In the next step, three DNA samples were created (2-3, 10 and 40 bp long chains) using low power focused laser beam by destroying some DNA molecules to give them unique structures. Subsequent resistance measurement revealed an increase of resistances of all three samples of DNA when an external magnetic field was applied while lowering the ambient temperature from room temperature to 0.05 K. However, proximity-induced superconductivity properties were noticed on two samples when their resistances decreased below the superconducting transition point of Re/C electrodes at 1 K. On the contrary, proximity-induced superconductivity properties were absent in 2-3 chain sample, which showed an increasing resistance even below 1 K. Kasumov *et al.* concluded that the resistance of DNA molecules does not increase with decreasing temperature and thermal hopping is least likely to be the mechanism for charge transport in λ-DNA.

3.5 Conclusion from the DNA Conductivity Experiments

From all the experiments described in the previous chapters, it can be concluded that the charge transport through short (≤ 40 nm) molecules is possible. All the measured currents through DNA were in the range of nano amperes, with the bias voltages in the range of 0.5 to 5 volts. This finding is consistent with the mechanism of coherent tunneling through a few base pairs and thermal hopping over a few nanometers. Also we can conclude that longer DNA molecules ranging from hundred nanometers to few micrometers are effectively insulating as

suggested by De Pablo *et al. [49]*, Braun *et al [50]*, and Storm *et al*. [46]. This can be interpreted as implying the idea that the DNA conformation is distorted by the force between DNA strands and the substrate and as a result, the π- stacking of the base pairs in long DNA strands is easily destroyed, thus the charge transport in DNA is blocked because of the disturbance.

To be more specific, the conditions of proper DNA conductivity could be broken down in two main criteria:

1. Differences in DNA molecules and their environments [45].
    a. To start with, the length of the DNA strand greatly influences the charge conduction for; DNA sequences with different base pair combinations posses different energy barriers for the charge to overcome which results in different electrical properties.
    b. The physical structure of the DNA molecules, such as in the form of ropes or in single molecule structure could also influence the charge conduction.
    c. Ions and counterions in the ambient environment can also play a big role in charge conduction because they tend to change the pathways for charge transport in DNA molecules.
    d. Changes in DNA structure (deformation) such as stretching will change the π-orbital stacking between the base pairs of DNA, thus changing the resistance properties of the molecules.
    e. The orientation of the DNA molecules (freestanding or surfacebound), sample preparation (use of different chemicals), ambient measurement conditions (humidity, temperature and thermal fluctuation of the solution) and different detection protocols are also important factors in DNA conductivity measurements.

2. The contact between the DNA molecules and the electrodes [51].
    a. When connecting the DNA molecules with a metal contact or with a substrate with linker chemistry, the physical contact should be ideally ohmic so that the measured conductivity is dominated by the DNA molecules and not by the interface.
    b. The contact is characterized by the nature of the tunneling barriers, as well as the work function of the electrodes [45].
    c. Some ambiguity still exists about the DNA energy levels, especially in the DNA LUMO (lowest unoccupied molecular orbital), at a DNA-electrode junction.
    d. In comparison with direct physical contact, chemical bonding between DNA and metal electrodes has been proved to be much more effective, as suggested by Xu *et al*.

To conclude, the DNA conductivity, or otherwise charge transport through DNA molecules is very much possible and a proven matter, however the above criterions must be met in order to have a successful DNA conductivity measurement.

CHAPTER 4

THEORY, EXPERIMENTAL PROCEDURES, DNA CONDUCTIVITY.

4.1 Theory

This chapter first explains the theory behind the use of nano-gap DNA detection sensor using functionalized gold nanoparticles in details. Then the detailed fabrication method of the nano-gap sensor is explained. In this part, some FESEM images are shown to give the reader a broad idea of the nanotechnology domain. Also, the functions of different micro fabrication machines that were used in this research work and their importance was discussed. Then the DNA attachment protocol with the silicon chip and explanation of the linker chemistry was explained, followed by the description of different types of chemical used, timing and ambient parameters. The most important part of the DNA attachment protocol is the DNA molar concentration calculation, because that suggests our detection limit and ultimately shows the sensitivity of the sensor. In the electrical detection of DNA part of this chapter, the current voltage (*IV*) measurement of the chip both before and after the DNA attachment was explained in details. The *IV* data shows efficiently the electrical detection of the DNA which was enhanced by Au nanoparticles. At the end in the result part, based on all the IV data and FESEM images both before and after the DNA attachment, a conclusion was derived about the experiment and the sensitivity of this DNA sensor. All the work described in this chapter such as chip fabrication, DNA attachment, FESEM imaging and *IV* measurements were done in the cleanroom and Nano-bio lab in the Nanofab center at University of Texas at Arlington.

Genetic mutation has long been proved to be the main cause of most cancers. Why mutation occurs is still a matter of serious debate; however researchers identified few well known sources such as sunlight, smoking and various types of radiation. Individual genetic

mutation or changes in DNA base pairs could lead a cell or tissue toward cancer. In many screening and diagnostic procedures, researcher identified mutated genes to be the main cause of different types cancer including hereditary cancer[52, 53]. In the last two decades, the main aim of cancer research has been the identification of different types of mutated genes that could be implicated as oncogenesis. As the result of extensive genetic research, it is now widely known that the alterations in DNA sequences are the main cause of the development of every neoplasm. These variations of sequences can be transmitted through the germline and can eventually result in susceptibility of cancer, or enhancing somatic mutation. Mutation in DNA sequence could happen because of simple copying errors that are introduced when DNA replicates itself; every time a cell divides, the entire DNA duplicates and results in two cells having full set of DNA. A gene is typically a sequence of the bases A, T, G and C that describes the type of protein they will evolve into. Any sudden change in this specific sequence can alter the gene's meaning and change the type of protein. There are many types of genetic mutations, and they are known as point mutation, frame-shift mutation, deletion, insertion, inversion and DNA expression mutation. The detailed explanation of these types of mutation is beyond the reach of this thesis; however, a strong case was made to show that the change in DNA sequence causes different type of diseases and it is very important to detect the specific changes in a sequence to correctly identify a disease.

4.2 Nano-gap DNA sensor

As specified in the previous chapters, it is very important to detect the base pair changes when mutation occurs in a DNA sequence to correctly identify a disease. Specific mutations in such genes can thus be used as diagnostic indicators for the susceptibility of disease, aiding in early detection and treatment [54]. There are various methods available to detect the presence or absence of particular genomic sequences. Microarrays are such a method which use single stranded DNA probes attached to chips (usually silicon) to capture fluorescently tagged genomic DNA where the fluorescent markers are excited for detection. In

addition to microarrays, a number of alternative detection mechanisms have been reported with the detection limits between a few nanomol and 1.8 fmol. They are: impedance measurements [28, 55, 56], capacitance detection [57], cyclic voltammeter measurements [58], and calorimetric measurements [59]. The microarrays and its fluorescent tags, however, can affect the stability and fidelity of the probe target interactions and could result in reduced reliability. Similarly all other methods described have major inherent limitations and the detection sensitivity is not that high. To overcome all these problems, this part of the thesis will describe an alternative probe detection method which uses functionalized Au nanoparticles and nano-gap electrodes to electrically detect the presence of medically mutant form of *K-ras* oncogene. Direct current measurements through the nano-gap electrodes show three orders of magnitude increase in the conductivity for the sample containing 2 femto-mol DNA molecules. Subsequently, FESEM imaging shows the successful DNA hybridization event for the perfect complementary (PC) chip.

4.2.1 What is K-ras oncogene?

The *Ras* family of oncogenes consists of three main members; *K-ras*, *H-ras* and *N-ras*, and all of these have direct implication in the development of human malignancies. The *K-ras* resides in the base 12 of the chromosome, and encodes a 21 KD protein, involved in the path of G-protein signal transduction. The mutation in *K-ras* is the main cause of over 90% of pancreatic carcinomas [60]. This constitutive activation of signal transduction pathway is the result of mutation in the *K-ras* oncogene which subsequently results in unregulated proliferation and impaired differentiation. About 30% of all human tumor is caused by the *Ras* family of gene mutation, and K-*ras* mutation are present in more than 50% of all colorectal adenomas and carcinomas; all because of the mutation at codon 12 of the oncogene [61, 62]. *K-ras* mutations are also the main causes of most common genetic abnormalities in pancreatic and bile duct carcinomas, which is present in more than 75% of tumors. Mutations at codon 12 are widely known to decrease the GTPase activity of *Ras* protein and disrupt their ability to bind at GAPs

sites, thus permanently maintain the activated state of *Ras* that promotes malignant cell transformation [63]. The mechanism responsible for high throughput of mutation in codon 12 is still unclear [64]. However, the detection of mutated *K-Ras* oncogene is of utmost importance in cancer diagnosis. Early and specific detection of these types of genes will enhance the treatment procedure and increase the chance of recovery.

4.2.2 Design of DNA Oligonucleotides

For this experiment, we specifically designed four different types of DNA oligonucleotides. They were named as Hairpin probe, PC (Perfect complementary) target, MM (Mis-match, 1 base pair) target and GNP (gold nano-particle) reporter. The DNA oligonucleotides used in this experiment were purchased from Sigma Aldrich (Saint Louis, MO). Table-1 shows the DNA sequences and their modifications.

Table- 4.1: Shows the sequences of each engineered DNA. Notice that the MM-target differs from PC-target by one base "G", which is the 5th base from left.

Sequence Name	Oligonucleotide (5` to 3`)	Modification
Hairpin Probe	AAAGGCAATTTCGCCGCCGCCATTGCC	5` C12 Amine
PC-target	GGC AAT GGC GGC GGC GAA	None
MM-target	GGC A**G**T GGC GGC GGC GAA	None
GNP-reporter	TGCCTTT	5` Thiol and GNP

The amine modifications were done on the 5` end of hairpin probe DNA for the linker chemistry, which attached the probe to the silicon dioxide surface. The GNP-reporter DNA also had 5` end thiol modification to attach gold nano-particles. We purposely designed the loop of the hairpin and one stem forming segment to be complementary to the DNA of interest. The loop part of the hairpin DNA is perfect complimentary to the PC- target. Also, the other side of the hairpin stem, starting from the bottom and seven bases up, is complementary to an engineered reporter oligonucleotide we named as GNP-reporter. Each GNP-reporter DNA strand is conjugated or chemically attached to a gold-nanoparticle. The hairpin probe consisted of a three nucleotide spacer, a 12 nucleotide loop, and a six base pair (bp) stem. Both the target DNA, PC-target and MM-target, were identical to each other except at one position (showed in

bold in Table-1). PC-target, the mutated version of the oncogene, was perfect complementary to the hairpin probe loop and one stem forming side. MM-target was the 18 bp wild type DNA taken from *K-ras* oncogene.

4.2.3 Electrical Detection of the Hybridization Event

The idea of electrical detection of the *K-Ras* oncogene stems from the concept of charge transport through DNA. To achieve this feat, same engineered hairpin probes were attached on three exactly similar chips. These chips had many pairs of isolated nanoelectrodes. The hairpin probes were specifically located between two isolated nano-gap electrodes. The silicon dioxide layer was grown on a silicon wafer to provide electrical insulation between the gold electrodes. The three chips were named as: PC chip, MM chip and control chip.

In the first step, PC chip was exposed to PC target, MM chip was exposed to MM target and the control chip was kept untouched. In the PC chip, the DNA of interest; the engineered perfect complementary PC target hybridizes to the loop, the stem of the hairpin probe destabilized and melted. Here, melting means the opening of the hairpin structure to become a long standing strand. Meanwhile, in MM chip, the 1 base pair mismatch MM target was unable to open and hybridize to the hairpin probe. Looking at this contrasting hybridization events from thermodynamic energy point of view, the probe DNA forms a strong hairpin loop structure with a stem size of six bp having ΔG_{probe} of –4.42 kcal/mol at 25 ℃ [65]. PC-target binds to the probe molecule with ΔG_{PC} of –24.45 kcal/mol. On the other hand, the calculated average energy of MM-target was ΔG_{MM} of –21.20 kcal/mol. The thermodynamic energies were calculated by using Gene Runner software. The reduced energy in the form of ΔG for MM fails to overcome the hairpin conformation, indicating hairpin structure has a lot more free energy barrier to overcome for a MM than what is calculated by standard formulas.

At this point, it is necessary to introduce the theoretical aspect of the energy calculation that was the backbone of engineered DNA design. The design of the hairpin probe, PC target and MM target hold the theoretical interpretation of this observed phenomenon.

It is a well known fact that if the complementary strand can be differentiated from a single-base mutant, then it can be much easily differentiated from multi- base mutant just by figuring out the base pair sequences. Now, let's focus on the equilibrium conditions associated with the PC and MM detection with the Hairpin probe. The equilibrium equations associated with PC and MM interactions with a hairpin probe in closed loop form (PR) can be written as $PC+PR \rightarrow PC_{duplex}$ and $MM+PR \rightarrow MM_{duplex}$ (with respective reaction free energies ΔG_{PC} and ΔG_{MM}) [58].

At equilibrium, the equilibrium constants for PC (K_{PC}) and MM(K_{MM}) can be determined by:

$$\ln K_{PC} = \ln([PC_{duplex}] / [PC][PR]) = -(\Delta G_{PC}/RT) \quad (3)$$

$$\ln K_{MM} = \ln([MM_{duplex}])/[MM][PR]) = -(\Delta G_{MM}/RT) \quad (4)$$

To quantitavely compare the selectivity by setting [MM]=[PC] = a , we get:

$$\ln [(PC_{duplex})/(PR)] = -(\Delta G_{PC}/RT) + \ln a = -(\Delta G`_{PC}/RT) \quad (5)$$

$$\ln [(MM_{duplex})/(PR)] = -(\Delta G_{MM}/RT) + \ln a = -(\Delta G`_{MM}/RT) \quad (6)$$

yields the energy criteria $-\Delta G_{PC} < 0$ and $-\Delta G_{MM} > 0$.

This model is directly verified with the introduction of GNP-reporter as a way to measure inability of MM to open the hairpin probe.

In the second part of the experiment, GNP reporter DNA molecules were introduced to all the chips. As explained previously, GNP reporter had sequences perfect complementary to the stem of the hairpin probe. Because of the successful hybridization events on the PC chip, the GNP reporter DNA got attached to the stem of the hairpin probe along with the gold nano-particle, which would eventually enhance the electrical detection of the hairpin opening. This phenomenon is conferred upon the system by the ability of the GNP-reporter to conduct electricity between the nanoelectrodes upon annealing to the exposed stem. The seven bases

GNP-reporter increases the detection limit of the system by increasing electrical conductance across the nanoelectrodes when the hairpin is in the open configuration.

Meanwhile in the MM chip, since the one base pair mismatch DNA, MM-target, was unable to open the hairpin probe, the GNP reporter would not on that chip. Around 8-10 percent of the GNP reporter would be on the surface of the MM chip due to physical attraction, and not because of the DNA hybridization. During the subsequent washing steps, most of the GNP reporter got washed away leaving most of the chip ineffective to the electrical detection. Similarly, the control chip also had very less amount of GNP reporter because of the physical attraction. Subsequent washing steps cleared away most of the GNP reporter DNA. It is important to notice that, the control chip also had hairpin probe DNA attached on it. The control chip behaved in a very similar way to the MM chip because both the chips got hairpin probe DNA in the original un-open position. As explained previously, this hairpin structure of the probe DNA makes this experiment very specific to the GNP reporter DNA. This approach can be used, in principle, to electrically detect any specific oncogene or mutation, thus paving the path for a very sensitive and highly specific label free DNA sensor.

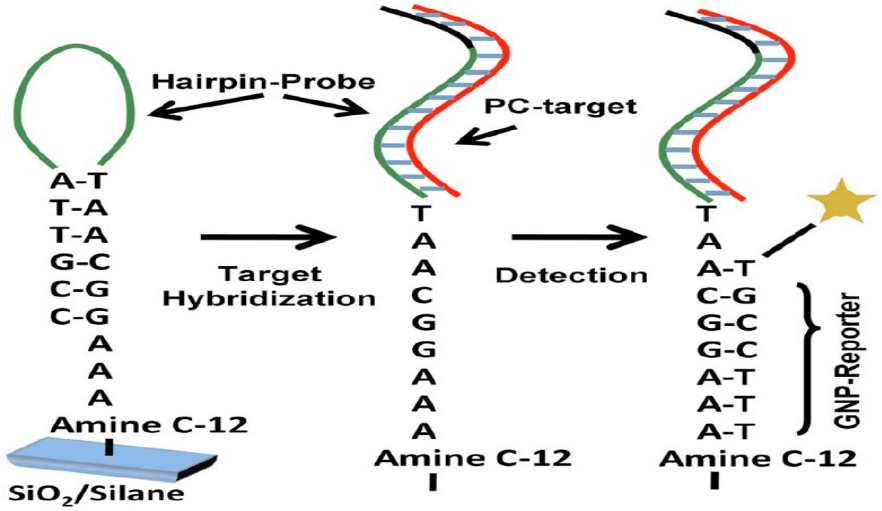

Figure-4.1: Schematic showing GNP reporter carrying gold nanoparticle (yellow star) binding successfully with hairpin probe after complementary DNA (PC-target, red) interacts with the loop (green) of the hairpin in “PC” chip. The PC-target starts with GGCAA and covers the whole loop. Black portion depicts the part of hairpin that formed the stem before opening.

The control chip was used to see the amount of Au nanoparticles got attached on the silicon dioxide in the absence of a DNA hybridization event. There will always be some physical absorption of GNP reporter DNA, however the amount would be significantly less than the case of successful hybridization. The sensitivity and selectivity of this sensor exclusively depends on the perfect complementary and mismatch hybridization scheme, where the Au nanoparticle only enhances the charge conduction through DNA. Before the actual experiment, few trial runs were done on bare silicon dioxide surface to get a rough estimate of the amount of Au nanoparticles to be expected. Here also three identical chips were used with similar hairpin probe DNA. The second step was done by flowing in PC-target, MM-target and no molecule on each of the identical chips. In the third step, GNP-reporter DNA was introduced to the chips and finally FESEM images were taken to see the amount of Au nanoparticles actually present on each of the chips. Interestingly enough, the results were on par of what was expected. FESEM images revealed a higher concentration of Au nanoparticles on PC chip surface compred to the other two MM and control chips. Later in the process, the amount of individual Au nanoparticles were manually counted using the software ImageJ and recorded for further evaluation.

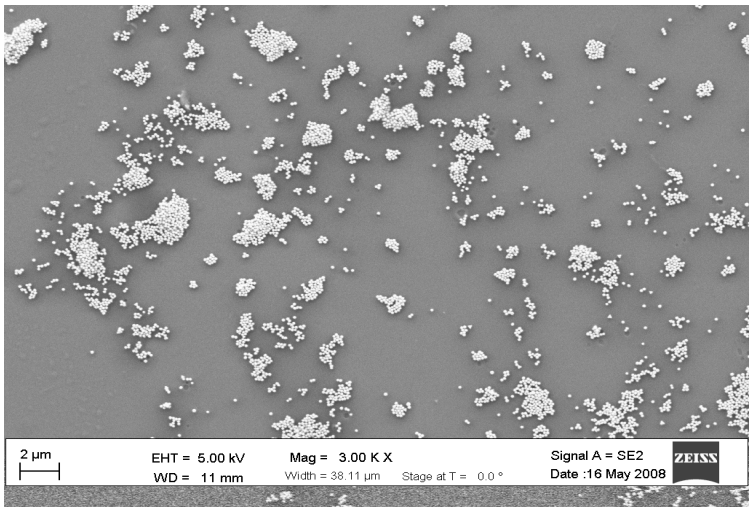

Figure-4.2: FESEM image showing the abundance of Au nanoparticles on bare silicon di-oxide surface as a result of successful DNA hybridization event.

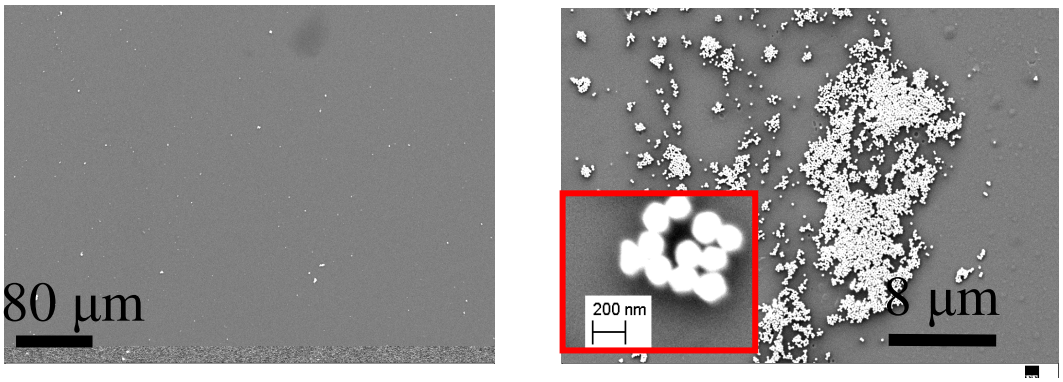

Figure-4.3: Side by side comparison of the amount of Au nanoparticles on MM (left) chip and PC chip (right).

4.3 Fabrication of Nanoelectrode Chip

The intricate design of the chip was done by using IC station software from Mentor Graphics. The design of the chip contained nanogap junctions along with continuous lines to create break junctions by electromigration. A two step lithography process was used to achieve the final structures. In both the steps, lift-off technique was used to get rid of the unwanted Ti/Au layers.

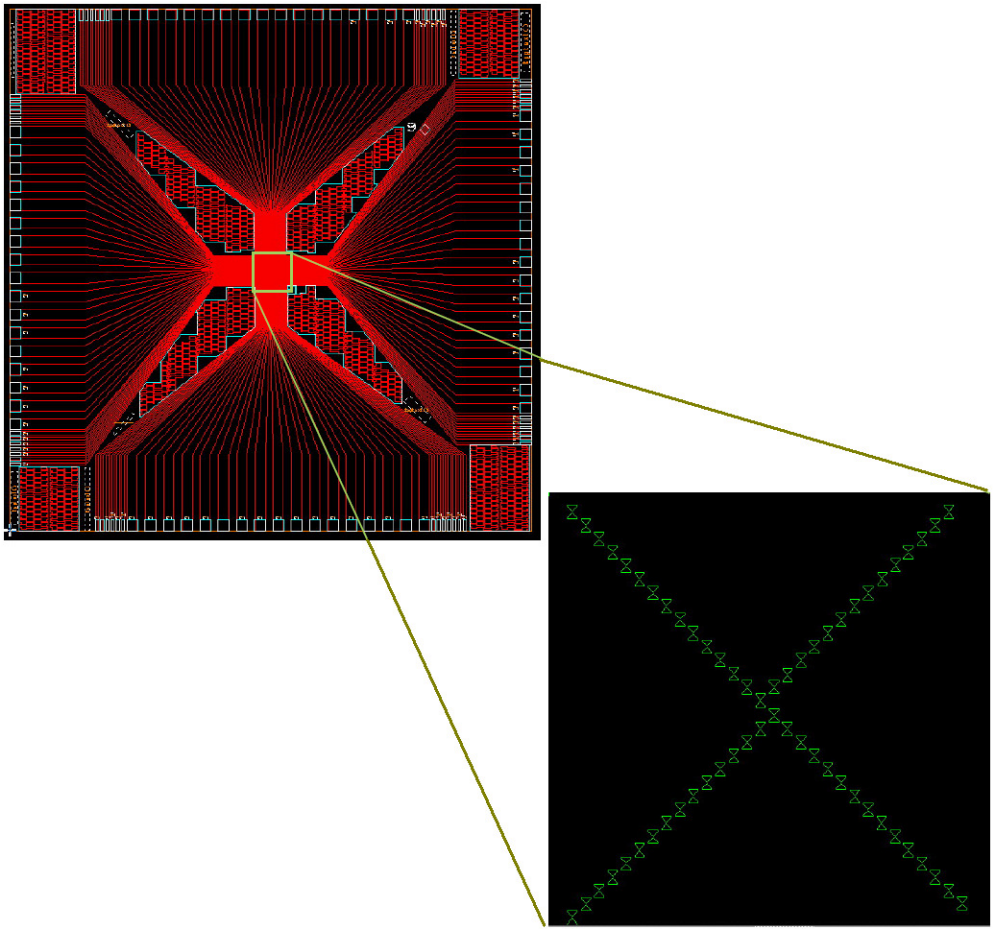

Figure-4.4: Schematic of line-type rendition of the Chip.

First, one µm of silicon dioxide was thermallu grown on p-type boron doped, <100>, 500 micron thick, 10-20 Ω cm resistivity and 4 inches diameter silicon wafer. Dry oxidation process was used to obtain good quality oxide to provide excellent electrical isolation to the nanoelectrodes. In the second step, e-beam lithographic process was used to pattern the wafer with positive e-beam resist PMMA (polymethyl methacrylate) followed by 50Å of Ti and 150Å of gold deposition by e-beam evaporation. The final pattern or the first layer was achieved by applying lift-off process to get rid of the unwanted metal. In the third step, optical lithography was used with conventional dark field mask to pattern for much bigger probing pads which

provided easy electrical pathways to the nano sized junctions. 100 Å of Ti and 500 Å of gold was deposited by e-beam evaporation followed by lift-off process to obtain the patterns in second layer. Extensive optical and SEM imaging was done afterward to make sure the fabricated structures depicted intended size.

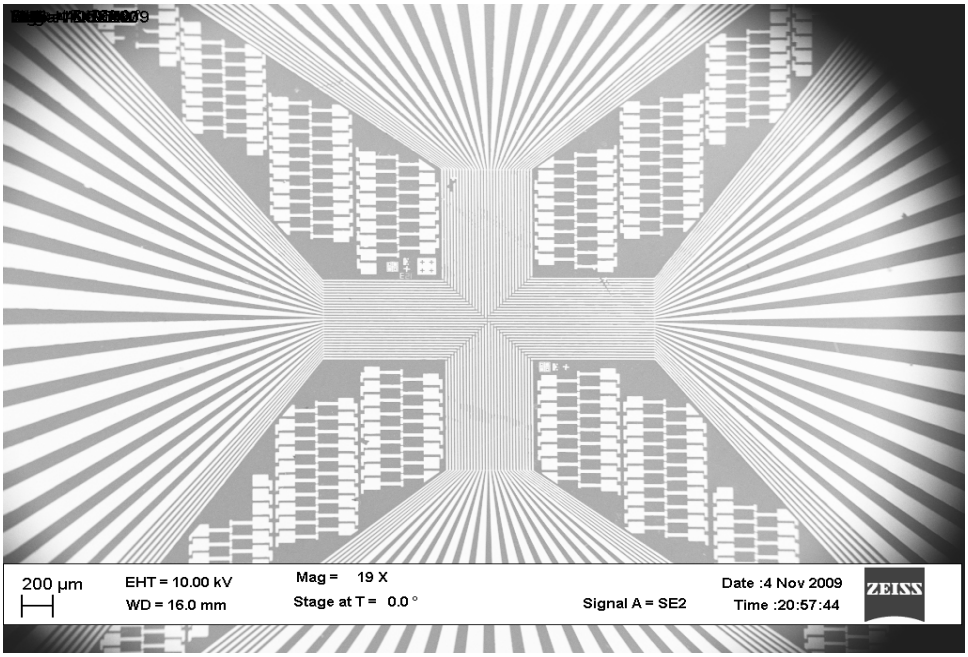

Figure-4.5: FESEM image showing the global view of the chip.

Following are some FESEM images taken at different parts of the final chip:

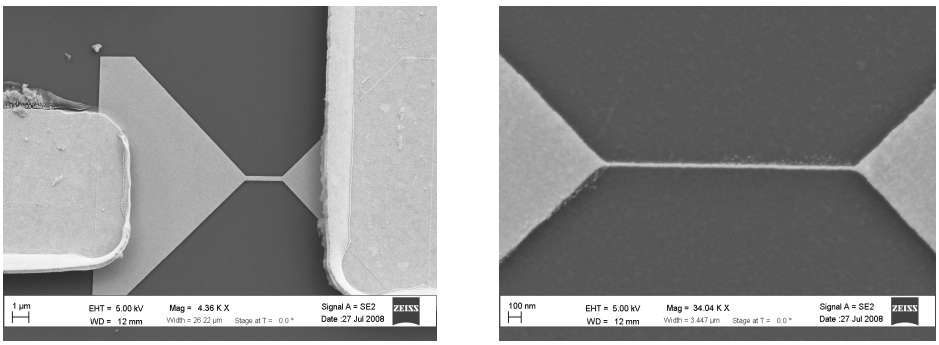

(a) (b)

Figure-4.6: (a) E- beam lithographed junction to make break junction by electromigration. (b)Nano-scale e-beam junction made for electromigration.

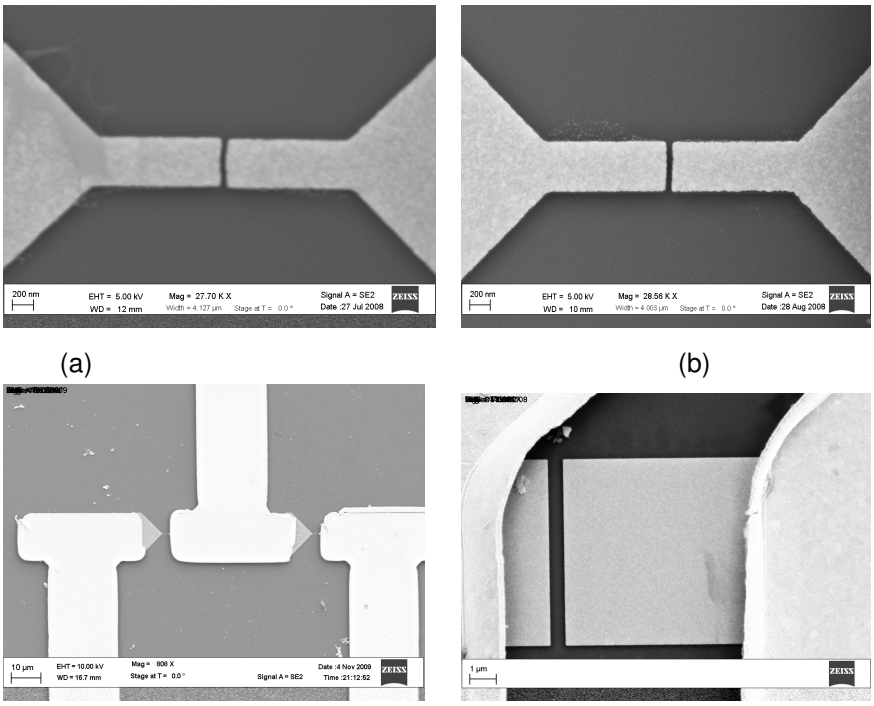

Figure-4.7: (a,b,c and d) e-beam lithographed nano-gap junction.

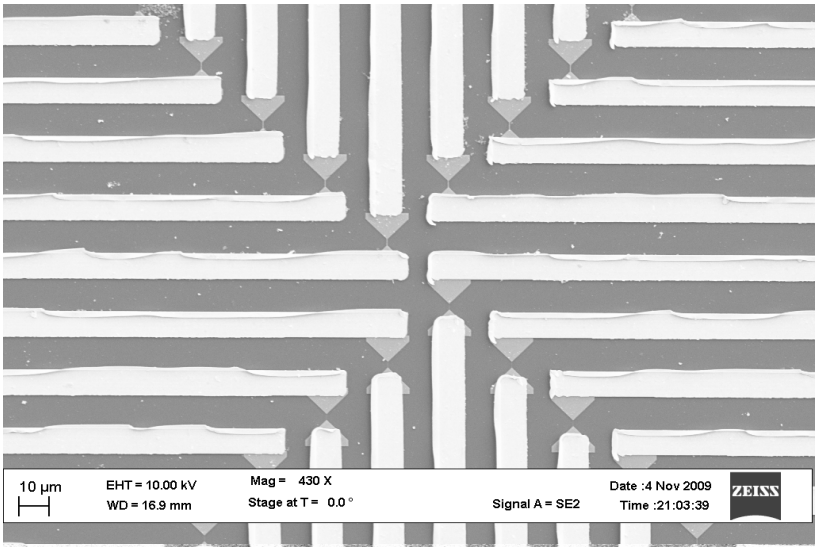

Figure-4.8: The center of the chip with all the different junctions.

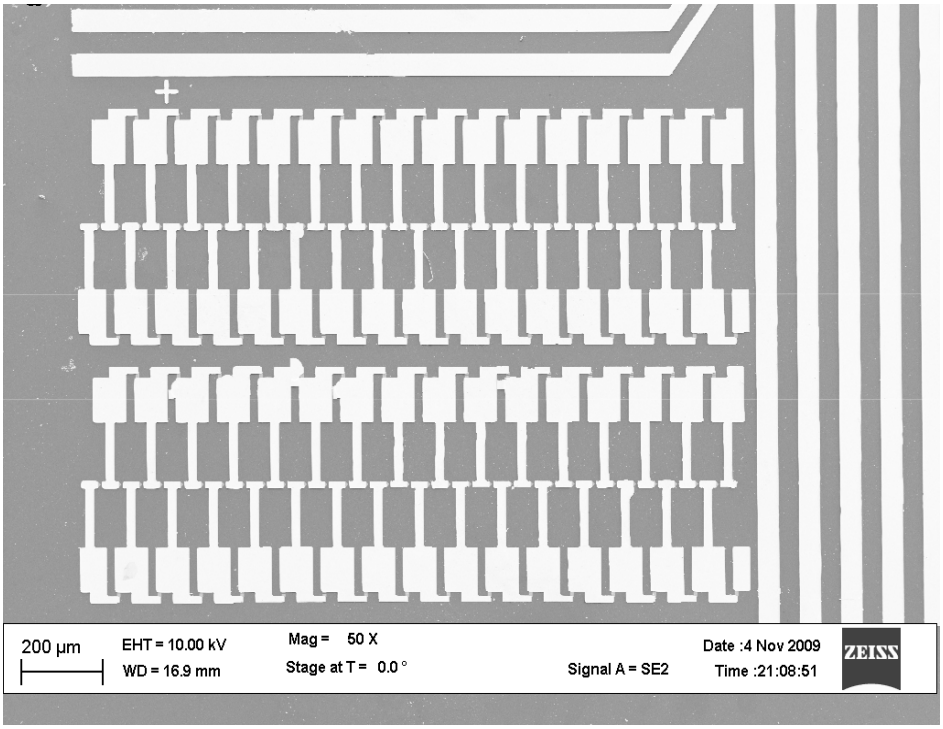

Figure-4.9: This structure is on all 4 sides of the chip.

4.4 DNA Attachment on the Chip

The DNA testing on the chip began with attaching hairpin probe DNA. In the second step, both PC and MM targets were introduced to the chips; PC target had complementary DNA sequences to the hairpin and successfully hybridized with it by opening it up, whereas the MM target had one base mismatch and was unable to open up the hairpin loop DNA. Then the GNP reporter DNA was introduced to both the chip. In PC chip GNP reporter successfully attached to the stem of the probe DNA. However, in MM chip, GNP reporter never attached. This was eventually detected by the surge of charge conduction in the electrical detection phase.

To attach the hairpin probe DNA to all three chips (PC, MM and control), first the chips were cleaned with oxygen plasma at 200 W in $Ar+O_2$ gas, then with Piranha solution. The purpose of oxygen plasma is to make the silicon dioxide hydrophilic, which introduces OH group to the oxide surface. Subsequent Piranha cleaning remove all the unwanted particles from the

surface. The chips were rinsed with deionized water and dried with abundance of N_2 gas. Then the chips were put in a nitrogen glove box with controlled ambience and temperature and the rest of the attachment process was carried out. A nitrogen glove box was designed and made from scratch in Nano-bio lab. The dimension of the box is 36 x 20 x 26 inches, and made from half inch thick acrylic sheet. The nitrogen glove box is connected with a vacuum pump and a nitrogen gas inlet. To create a controlled environment inside the box, first the vacuum is turned on to pump out all the ambient air inside. Then the nitrogen is released inside the box. This process is repeated twice to make sure all the ambient air is gone and only pure nitrogen gas is present inside.

Silanization was done in a solution containing 5% 3-Aminopropyltrimethoxysilane (APTMS) solution with 95% ethanol. The Chips were then incubated in the APTMS solution for 12 hours at room temperature inside the nitrogen glovebox. After silane functionalization was done, the chips were rinsed with ethanol and deionized water and cured at 110 ℃ for 15 minutes in a fan-operated oven. To activate the surface for DNA attachment, the silanized chips were immediately immersed and kept for 24 hours in 1 mM 1,4-Phenylene diisothiocyanate (PDITC) dissolved in dimethylformamide (DMF) containing 10% pyridine. The chips were then washed with DMF and 1,2-dichloroethane and dried with notrogen. Each activated chip was immediately immersed in 2 ml of the hairpin probe DNA solution. The substrates were incubated in DNA solution at 37 ºC for 72 hours. The vials were gently shaken after every 24 hours. After DNA attachment, the substrates were washed with deionized water and ethanol, and dried in gentle nitrogen flow. The surface attached probe molecules were heat cycled in TE buffer three times to ensure all molecules formed hairpin loop structures. To deactivate the unreacted surface-bound isothiocyanate groups, the chips were immersed in a blocking solution of 50 mM 6-amino-1-hexanol and 150 mM DPEA in DMF for 2 hours after which the substrates were sequentially washed with DMF, acetone, deionized water and dried in the stream of nitrogen.

The GNP-reporter conjugates were prepared using thiol-gold chemistry as reported in Storhoff *et al.* [66]. Then in the next step, the PC chip was immersed in TE buffer (pH 7.4) containing PC target DNA, and the MM chip was in 1 base pair mismatch MM target DNA for 24 h at 40 °C. Both PC and MM-target had a DNA concentration of 2 fmol/µl. The chips were then rinsed with methanol and de-ionized water. Chips were then incubated in TE solution containing GNP-reporter. The GNP-reporter got bound to the stem region of the probe toward the chip surface when it became available on binding of PC with probe (and was unavailable otherwise). In addition to the "PC" and "MM" chips, the control chip was also gone through the following procedures: (1) probe-functionalized chips not exposed to any target and (2) chips lacking probe and exposure to target DNA (i.e., silane SAM surface chemistry only). The control chip was then incubated with GNP-reporter sequence as above. In the subsequent testing, the control chip did not show any attachment of the GNP-reporter sequence.

Now all the three chips are ready for *I/V* testing in Semiconductor Parameter analyzer.

CHAPTER 5

RESULTS AND DISCUSSION

After all the DNA attachment and GNP reporter hybridization process were done, all three chips went through electrical measurements. For this purpose, an Agilent 4155C semiconductor parameter analyzer was used.

It is very important to note that, before the DNA attachment on the chip a first round of probing was done on all the nano-gap chips to see the electrical conduction properties of each pair of electrodes. The chips were placed on probe station connected with Agilent 4155C, and then probed on each and every individual probing pads. Two micromanipulators were used to probe on each side of the nano-gap junction and a voltage was swept from -1 to + 1 V. For the breakjunction electrodes, a voltage was swept from 0 to 5 V to create junction by electromigration.

5.1 Conduction before DNA Attachment

When each nano-gap junction was probed and a voltage sweep was applied from -1 to 1V, 95% of the nanogap junction showed no form of charge conduction. The *IV* data showed only noises.

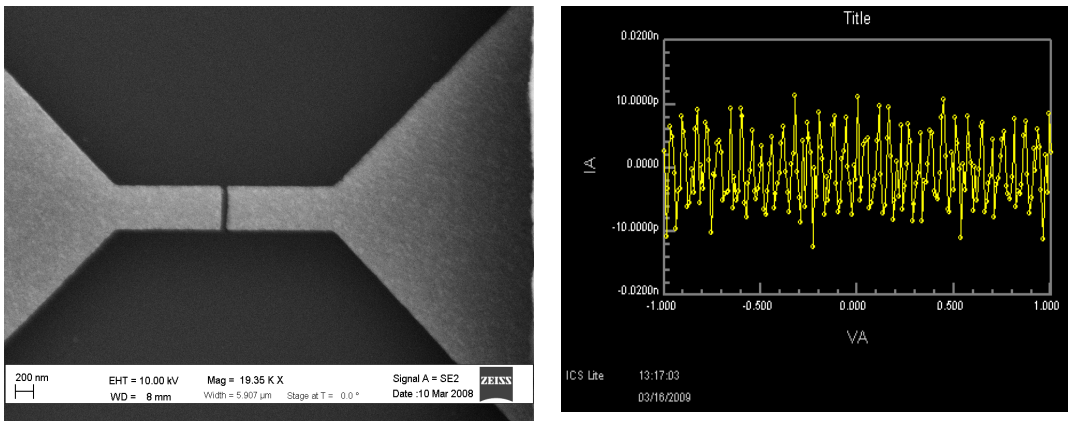

(a) (b)

Figure- 5.1: (a) showing the nano-gap junction and (b) showing the screenshot of the *IV* data when a voltage was swept from -1 to 1 V. The image on (b) represents only noises showing zero charge conduction.

As previously mentioned in the chip fabrication part, some junctions were fabricated as continuous Au lines to create break junctions by electromigration. In order to carry out this process, a voltage sweep was applied from 0 to +5 V and the *IV* plots were recorded. With the increase of voltage, more electrons conducted through the Au line and they interacted more with the imperfections in the metal line. Meanwhile because of this rush of electron flow, the thermal energy also increased and at one point, failure occurs in the physical layer of the metal. This phenomenon is commonly known as electromigration. In this case, the semiconductor parameter analyzer *IV* plot was real time, which gave a clear voltage and current reference to exactly where the failure was happening. Interestingly, almost all the break junctions were created at a particular current, which shows uniformity of the Ti/Au layer across the chip.

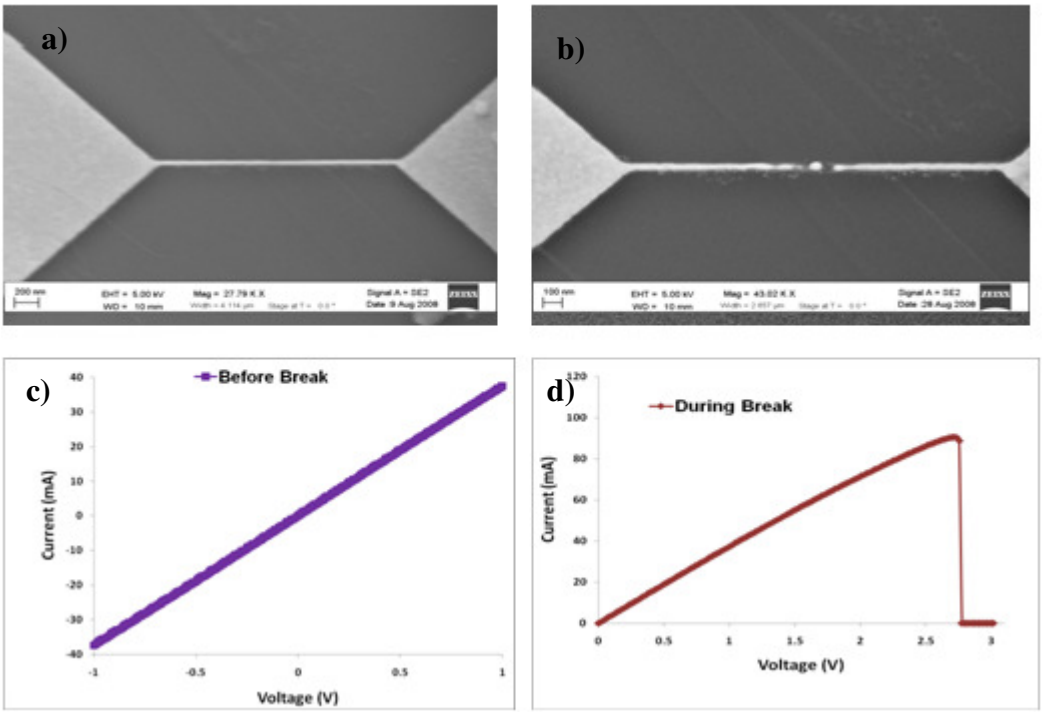

Figure-5.2: (a) Junction before electromigration. (b) Junction after electromigration. (c) *IV* plot of break junction before electromigration and (d) *IV* plot showing the ramp in voltage and the point of electromigration.

Similar probing and electromigration technique was used in all three chips and all the data was recorded. The *IV* data's were then converted in excel sheets, having three columns. The first column was for sweep voltage, second one for the passing current and the third one for resistance calculation, which were V/I. Then the excel sheets were grouped in two categories for each chip, before DNA attachment and after DNA attachments. Matlab was used afterward to process the entire data file and the *IV* data was plotted in for each chip. The final graphs for each chip included the before and after DNA attachment IV plots for easy comparison.

5.2Conduction after DNA attachment

After the DNA attachments and the hybridization process, all three chips were tested for charge conductivity in the probe station again. Probing the same way as before, a set of new data was recorded for the PC, MM and control chip.

In the PC chip, a total of 120 nanogap and break junctions were probed to obtain electrical conductivity data in the form of *IV* plots. Among them, 96 junctions showed a robust increase in charge conduction, which is approximately 80% of the total junctions exposed to PC target. In further analysis, it was found that the resistance was reduced by three orders of magnitude. A matlab code was developed to plot the *IV* data for before and after DNA attachment in one graph.

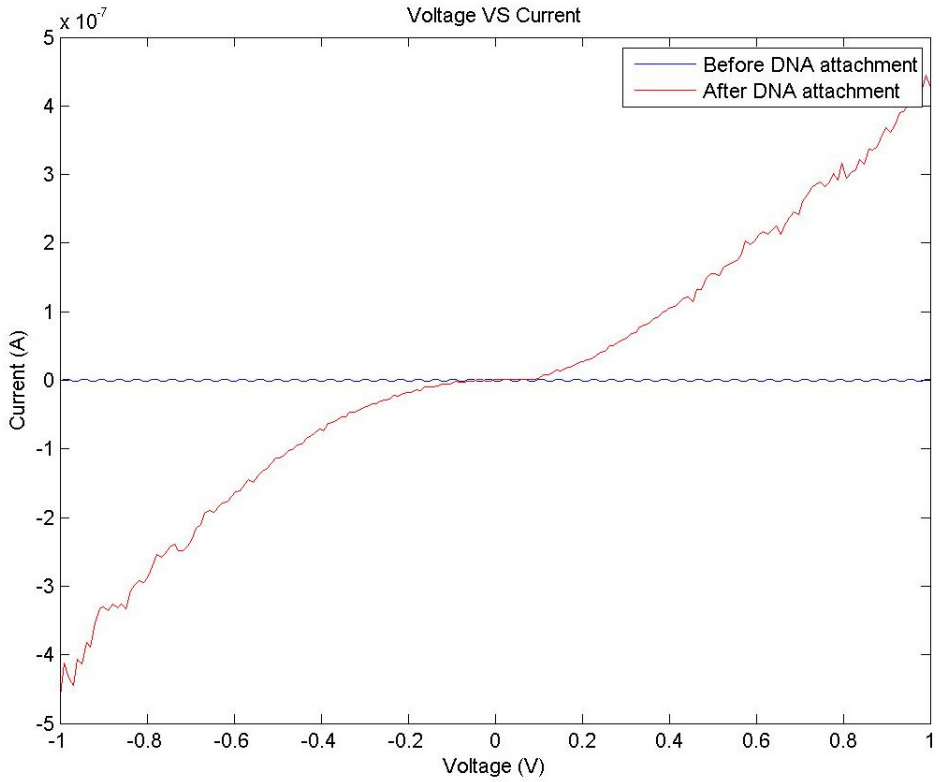

Figure- 5.3: *IV* plot of the PC chip after DNA attachment. All 96 junctions out of 120 showed similar responses.

This increase in charge conduction was due to the presence of GNPs in the PC chip because of successful hybridization event, which provided easy path to charge-hopping sites to the carriers, This process is acting as a transduction block for the binding of PC with the probe. The tunneling current is taking an intricate path of DNA and GNP when traveling through the

nanogap or the opening of a break junction. The tunneling current in this network of GNPs and DNA in a system of the nanogap electrodes with insulator (vacuum) between them can be approximately described by the Simmon's formula.

To briefly describe Simmons formula:

$$J = (\frac{\alpha}{\delta_z^2})\{\bar{\varphi}\exp(-\mathrm{A}\delta_z\sqrt{\bar{\varphi}}) - (\bar{\varphi} + eV)\exp[-A\delta_z\sqrt{\bar{\varphi} + eV}]\} \quad (7)$$

Where $\alpha = \frac{e}{(4\pi^2\beta^2\hbar)}$, $A = 2\beta\sqrt{\frac{2m}{\hbar^2}}$ (8)

and φ is the average barrier height relative to Fermi level of the negative electrode, δ_z is the barrier width, and eV represents the applied voltage across the nanoelectrodes [67]. β is the dimensionless correction factor, e and m are the charge and mass of electron respectively, and $\hbar$ is Dirac's constant. At small voltages when $\varphi \gg eV$, the Simmon's formula simplifies as

$J = (\gamma\sqrt{\frac{\bar{\varphi}V}{\delta_z}})\exp(-A\delta_z\sqrt{\bar{\varphi}})$, where $\gamma = \frac{(e\sqrt{2m})}{(4\pi^2\beta^2\hbar)}$

In the case of small voltages, the barrier height $\bar{\varphi}$ becomes independent of the applied voltage and the tunneling current becomes linearly dependent only on the applied voltage [68]. The tunneling current characteristic can thus be modeled as two electrodes with high resistance between them. As the PC-target binds between these electrodes and GNP-reporter brings in GNPs, electrons find a lower barrier and thus start tunneling efficiently. Such framework shows the potential of electrical conductivity in microarrays. The measurement of this electrical conductivity, or otherwise the tunneling current is very critical due to the signal to noise ratio. Measuring current in the range of mA to μA with high signal to noise ratio is quite challenging without any sort of signal conditioning. High impedance analyzer such as semiconductor parameter analyzer with built in signal conditioning on the output signal was effectively used for all the measurements. The tunneling current sometime can be really unstable due to the

ambient parameters such as humidity, temperature and vibration, which gives a sudden peak to the signal to noise ratio.

In the MM chip, after probing all 120 nanogap and break junctions, only 9 of them showed some sort of increase in charge conductivity. The current-voltage (*IV*) measurements on MM chips showed a slight increase in conductivity all within the same order of magnitude, and even that followed no pattern like the PC chip. The percentage of increased conductivity in MM chip is approximately 8% compared to 80% of the PC chip. This proves how well our theory worked in the real experiment and the accuracy of our DNA design.

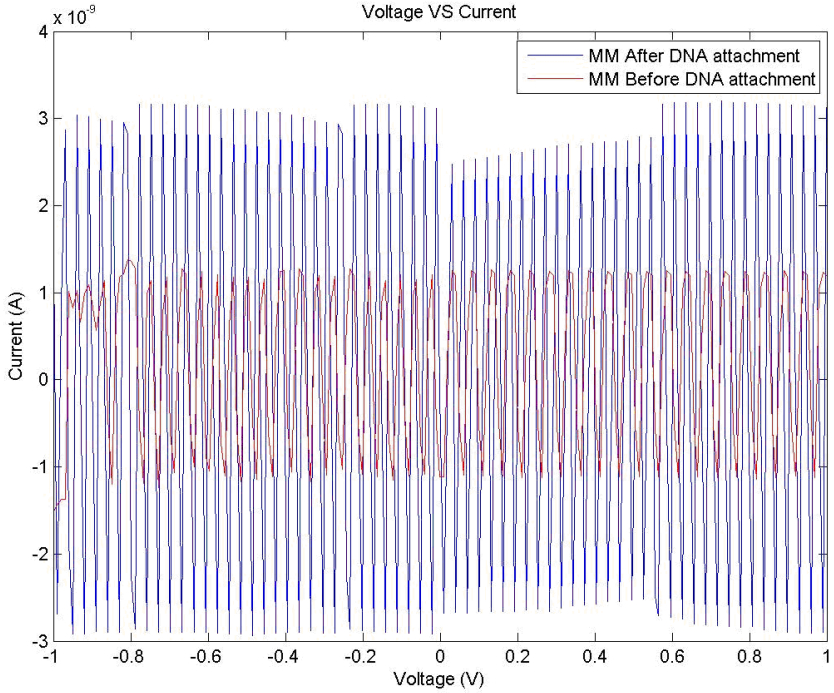

Figure-5.4: The *IV* plot of MM chip both before and after DNA attachment.

Similarly on the control chip, the *IV* measurement was done both before and after the DNA attachment. The IV data showed almost identical behavior of the control chip compared to MM chip. Since the control chip only had hairpin probe and it was not exposed to any other DNA, the hairpin structure stayed intact. When exposed to the GNP reporter, the control chip

behaved similarly to the MM, because the GNP reporter DNA did not have anything to bind to and hybridize. Some GNP just got attached on the chip due to physical adsorption.

To reinforce our theory of electrical detection, each and every junction of PC, MM and Control chip was imaged with FESEM. It is important to note that, all the junctions were also imaged before the DNA attachment to provide a clear comparison of visible Au nanoparticles. After complete imaging on PC and MM chip, the visible Au nanoparticles were counted by imageJ software.

The SEM imaging and data provided by ImageJ software revealed a clear distinction between PC and MM chip, and also confirmed the validity of the *I-V* measurements. The images showed clusters of GNPs on PC-target chips between the nanoelectrodes, which provided the pathways for increased current through otherwise insulating electrodes. SEM micrographs also showed a negligible number of GNPs on the surface of MM-DNA chips. The few GNPs on the MM chips can be attributed to physical adsorption.

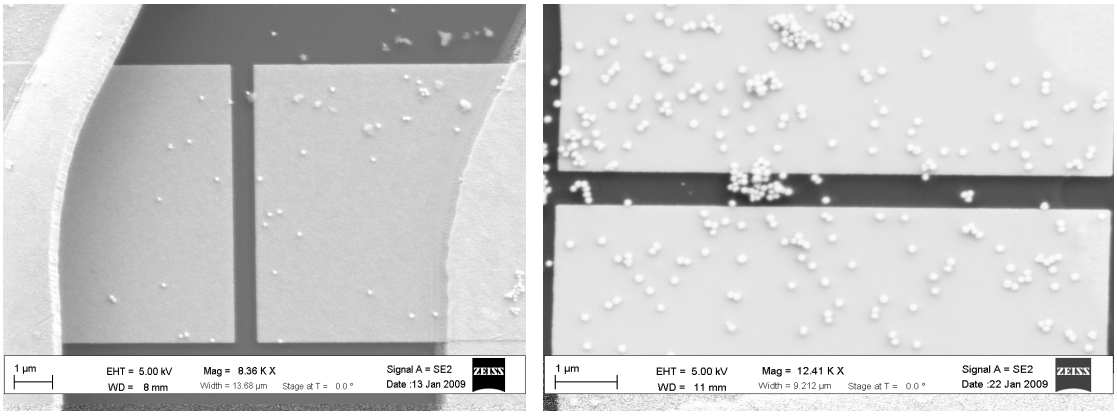

(a) (b)

Figure-5.5: (a) SEM image of MM chip. (b) SEM image of PC chip showing much higher concentration of GNP as the result of successful hybridization events.

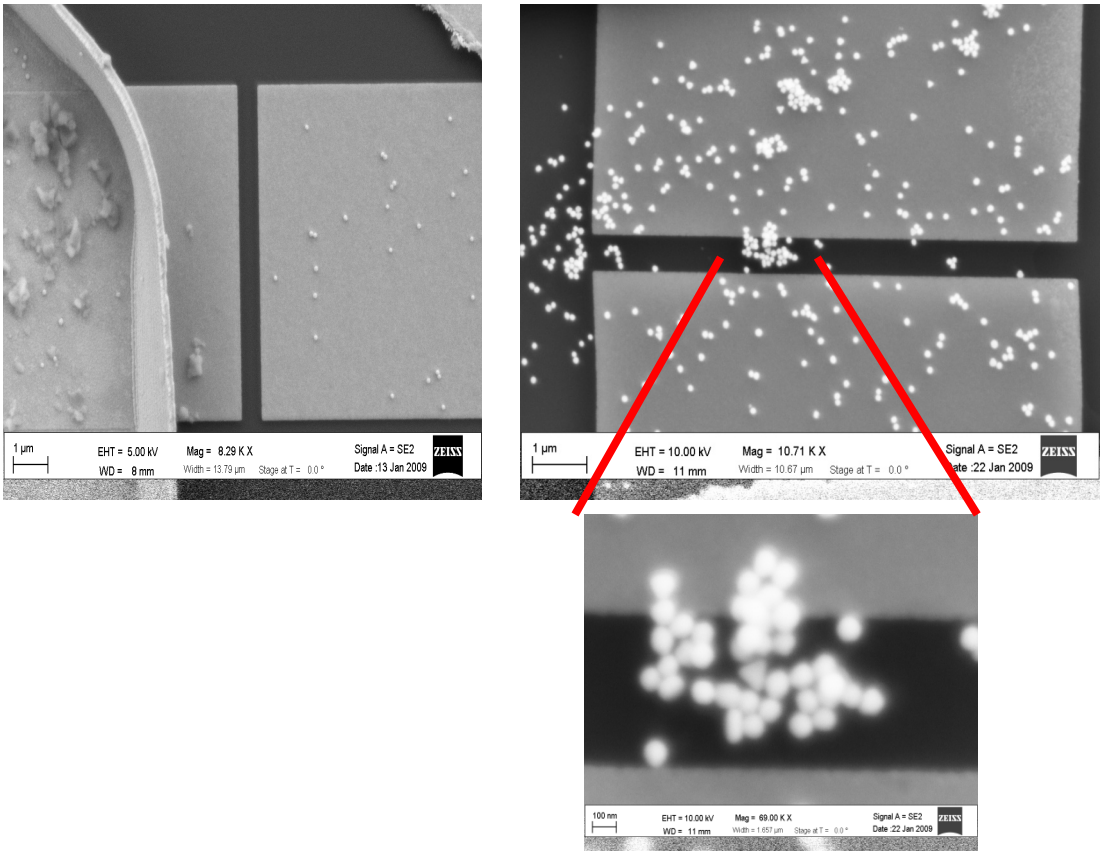

Figure-5.6: Another SEM image of nanoelectrode chips showing side by side comparison of the amount of GNP in case of MM-target (left) and PC-target (right). There is a distinct difference in the GNP densities. Inset to right image shows closeup images of GNPs bridging the gap between the nanoelectrodes, causing the increase in conductivity for PC-target.

Additional to the visual confirmation by SEM images, the average count of nanoparticles on silicon surface was obtained with the help of high resolution SEM imaging and ImageJ software, and the numbers of Au nanoparicles were counted per μm^2. From this data, the percentage and standard deviation of Au nanoparticles present per μm^2 were found for PC and MM chip. This is another strong evidence to differentiate between the PC and MM chip. Table-2 gives the extracted data.

Table-5.1: Count of average number of Au nanoparticles per μm^2 on silicon.

DNA Complexes	Mean number of particles/μm^2	Standard deviation
Hairpin Probe+PC-target+GNP-reporter	11.62	5.60
Hairpin Probe+MM-target+GNP-reporter	0.86	0.76
Hairpin Probe+GNP-reporter (Control)	0.10	0.09

The PC data both before and after DNA attachment showed three order increase in conductivity (Figure.5.7). This concluded that the increased in electrical conduction was due to the successful hybridization process of the PC DNA whereas the MM electrical data showed an unsuccessful hybridization event. This means that we can design our chip to electrically detect any kind of DNA sequence, consequently detecting a virus or disease.

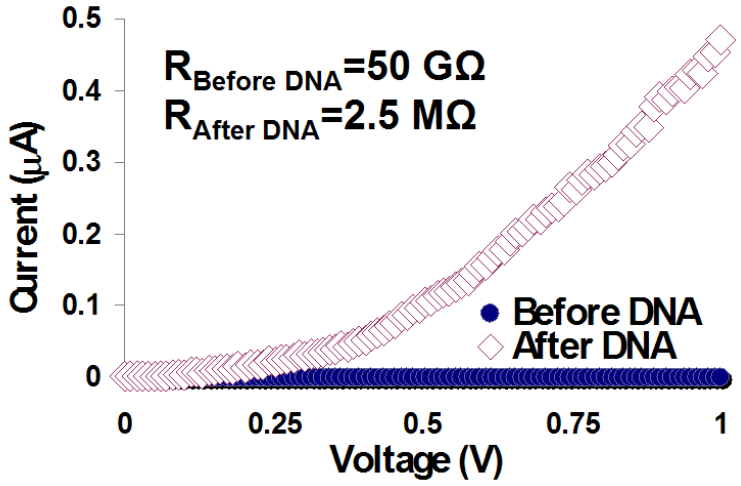

Figure-5.7: Comparison of *I-V* data for a representative nanogap before hybridization of PC-target and probe (circles) and after exposure and hybridization of probe to PC-DNA and GNP-reporter (triangles). The average change in resistance before and after DNA attachments also shown on the figure.

5.3 Conclusion

In this thesis, the electrical properties of DNA were employed for an application in DNA sensing. The experiments showed that even a single base pair mismatch in the DNA sequence is possible to detect electrically. The process described here has very high specificity and sensitivity, and these two characteristics are very important in the development of a sensor.

First, all the background information was gathered about DNA conductivity and the possible reasons for it to act otherwise. Careful research was done to find out the characteristics of single strand and double strand DNA in the case of long and short range charge conduction. Then, the DNA molecules and hybridization process was designed in such a way that the difference is minimum between two almost identical DNA sequences. Only one base pair mismatch would determine the successful hybridization process, hence detecting the DNA molecule electrically. An elaborate protocol was also devised to attach DNA on the Si/SiO_2 substrate.

Next, using MEMS and nanotechnology, we fabricated nanogap electrodes and attached DNA. In subsequent steps, we introduced unique DNA molecules called PC, MM and GNP reporter to melt and hybridize DNA strands and used Au nanoparticles to amplify the electrical signals when probed to obtain charge conduction data. In the electrical detection process, the DNA-of-interest target molecules were electrically detected using engineered hairpin probes. The detection of hybridization events were successfully amplified by using a GNP-reporter sequence complementary to stem region of the hairpin probe. The presence of GNP between electrodes enhances the conductivity between otherwise insulated nanoelectrodes. The GNP-reporter can be modeled as a circuit breaker demonstrating electrical quantification of the molecular interactions. The device has the potential to function as a traditional microarray but without the need to directly tag either the probe or target molecules.

The main purpose of this thesis is to show the electrical detection of even a single base pair mismatch is possible and how this concept can be applied to make a label-free DNA sensor. As previously stated, DNA has specific electrical properties and it does acts pretty much like an electrical component depending on certain ambient conditions, length and how it is connected to the electrical circuit. Almost all experiments described in this thesis were done with nanogap electrodes and break junction (suitable for its Josephson tunneling properties). So it can be easily concluded that nanogap electrodes can be used as a sensor to detect DNA parameters and sequence specific information.

CHAPTER 6

FUTURE WORK

The research work of electrical detection of DNA and its implication in bio-chemical sensor field described in this thesis holds many advantages over conventional microarray and other state-of-the art technology available nowadays. However, there are still lot of works needed to be done to exploit the full potential of this technology. As explained in the previous chapters, the nanogap electrodes method of DNA detection has very high sensitivity and specificity, and the process is less time consuming compared to other methods. Also the novel method of designing probe DNA and ss-DNA with specific selectivity could be used for point mutation for different disease detection. Further innovations are already in the picture to make this process highly cost effective and a packaged product which can be used as a point-of-care device for faster disease detection. The following sections in this chapter will provide few future directions to integrate different technologies for a very efficient point-of-care diagnosis device.

6.1 PDMS nano channels

In the nano-bio lab (NBL) at University of Texas at Arlington, lot of innovations were done in the field of nano fluidics and new techniques are being developed to efficiently produce PDMS nanostructures. Though still in research and development stage, researcher in nanobio lab has devised a unique technique to make nano scale channels in PDMS block with active filtration system without the use of conventional lithography techniques. These channels hold enormous potential in targeted drug delivery and DNA/RNA detection. With further refinement in techniques, these nano channels can be fabricated to deliver bio samples to a specific site in 10-20 nm range. Thus a PDMS block with nano channels attached on top of a nano electrode chip would enable the efficient delivery bio samples to a specific site or to a specific electrode

pair for a specific detection. Using this technology would pave the path to use a single chip for various disease detection without the possibility of contamination of bio samples. Site specific DNA binding with different probe DNA will send out *I-V* data to notify the presence or absence of the disease.

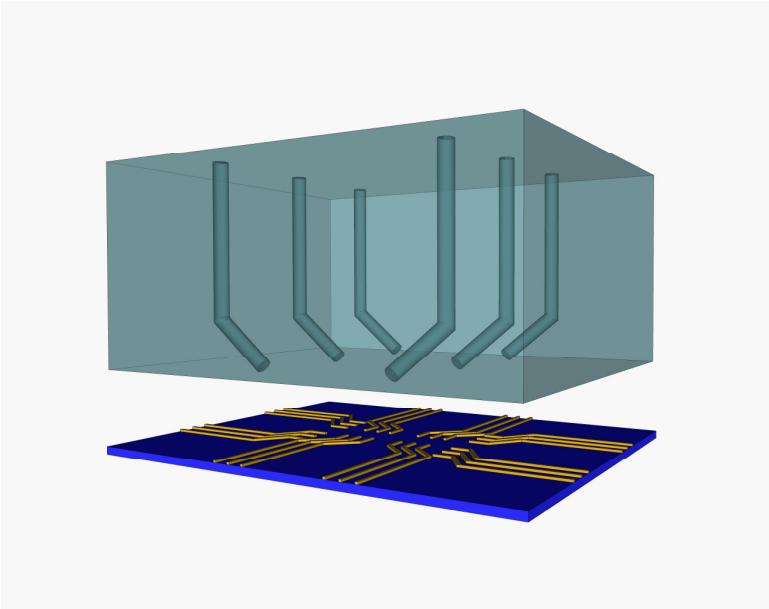

Figure- 6.1: PDMS block with micro channels to be attached on top of the chip.

6.2 Using Labview, DAQ Card and Digital DMM to Replace SPA

All the *I-V* measurements described in this thesis were done by Agilent 4155C SPA (semiconductor parameter analyzer). This SPA provides extremely accurate laboratory bench top solution for advanced device characterization. It has low-current and low-voltage resolution and built-in quasi-static CV measurement capability. However, this SPA is very expensive (in the range of $50,000) and the huge form factor makes it inconvenient to integrate with a point-of-care chip. Keeping this in mind, an innovative *I-V* measurement device was put in place at NBL. Using a National Instruments data acquisition card (6070E Multifunction I/O) and a high precision digital multimeter (NI PXI 4071) in an external PXI chassis(NI PXI 1033) connected

with a PC, a system was developed to measure the *I-V* data of nano electrode chips. The idea is to provide sweeping voltage by the DAQ card and measuring the current across the nano electrodes by the DMM. This system is controlled by Labview software and an efficient GUI enables to changes the *I-V* parameters as needed. The PXI chassis is connected with an external output box with numbered ports. For future innovation, the actual nano electrode chip could be wire bonded to a flip chip package and connected to the output box for efficient *I-V* measurements. This way, an extremely versatile POC device could be achieved with a price tag of around $3,000.

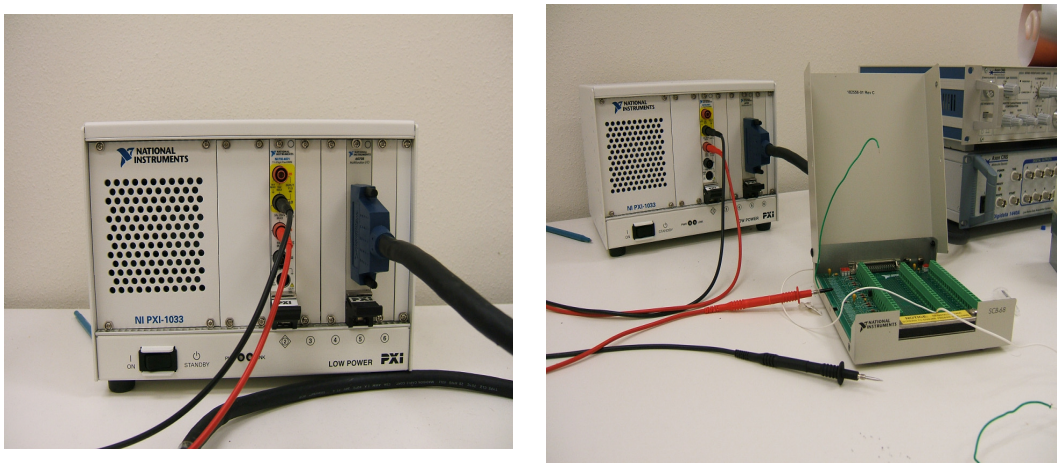

(a) (b)

Figure-6.2: (a) The DMM and DAQ card in the PXI Chassis. (b) PXI chassis with the external connector box.

6.3 Using a DEMUX for Efficient Switching

During the course of this experiment, all the *I-V* data taken from the nano electrodes chip was done by manual probing to each and every individual electrode pairs. This method is acceptable for research or for proof of concept, but not for a point-of-care device. For this reason, future innovation on this chip needs automatic switching of *I-V with* single input and output. This can be achieved with the help of a DEMUX and a surface mount chip carrier (IC package). A demux (demultiplexer) is a device which takes a single input signal and digitally splits in one of many output lines. This split or switching to one of many data output lines could be easily controlled by a set of algorithms. By changing the binary values, it is possible to address each and every individual nano electrodes and obtain *I-V* data. Demux is easily programmable by labview software and a single GUI could be use to control all the parameters.

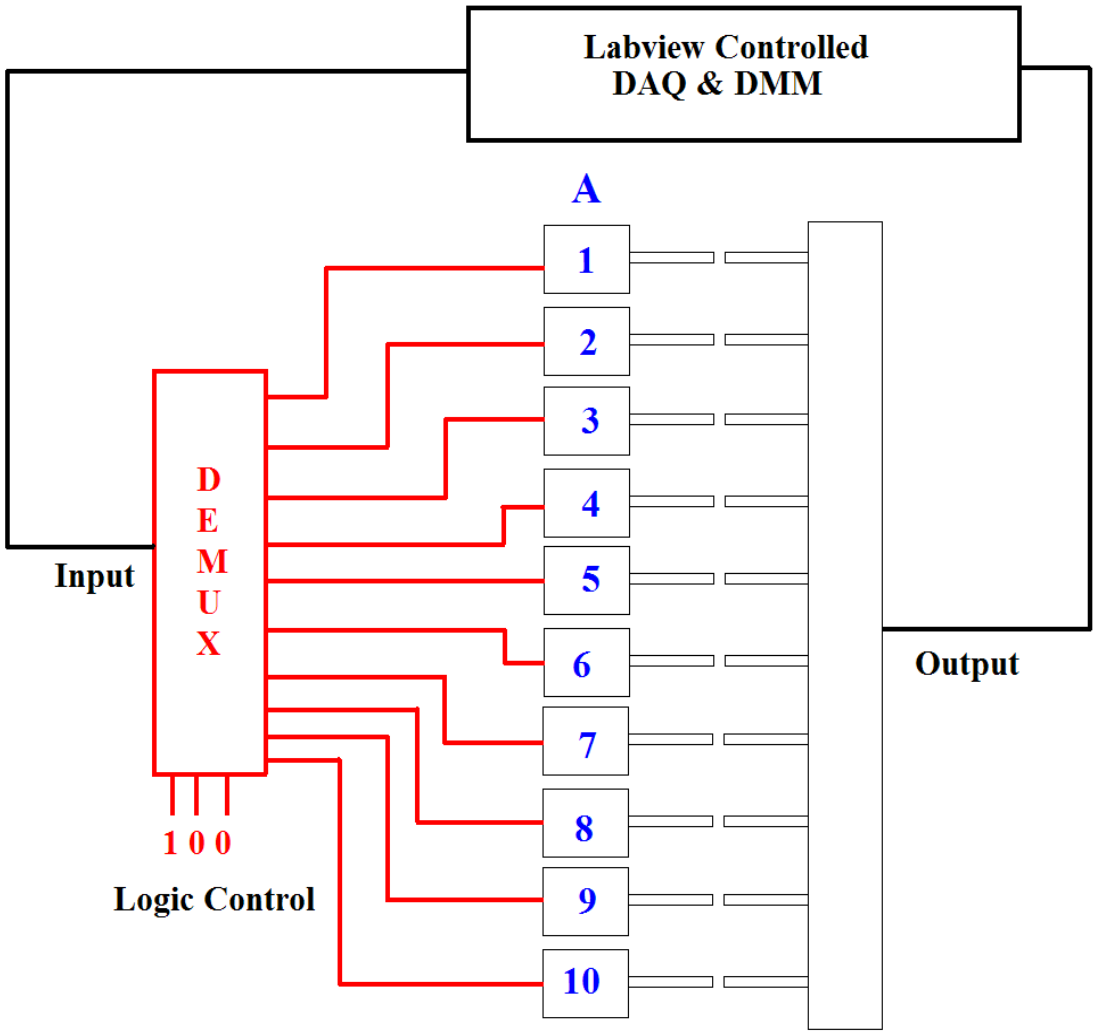

Figure-6.3: Schematics of the Demux controlled nanogap electrode chip.

6.4 Integration with LDCC Surface Mount Package

After the integration of Demux, the assembly could be placed on a surface mount chip carrier package and wire bonded at the output and input. Depending on the number of nanogap electrode pairs, different LDCC (Leaded Chip carriers) are available in the market and the integration can be done in minimum amount of time. LDCC packages are basically area array packages, which mean the connecting leads are on the edge of the package. The LDCC packages are extremely popular because of reliability and ease of use. Some of the advantages of LDCC packages are given below:

- High performance and thermal reliability
- Easy to mount on PC board via socket, manual wire bonding or automated equipment
- Easy to solder and reliable removal techniques
- Lead spacing matches common PC Board layouts and allow one or more leads to run between the PC Board holes
- Effective heat dissipation
- Hermetically sealable using solder, glass or epoxy

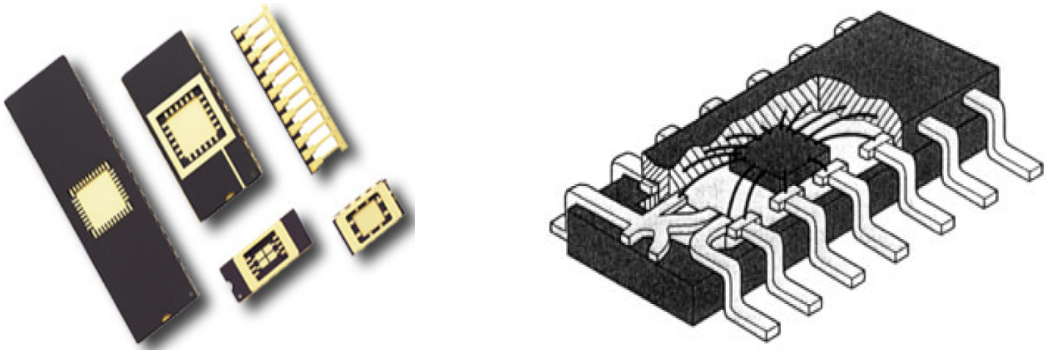

Figure-6.4: Images showing different kind of LDCC packages [69].

After the process is complete, the DNA electrical conductivity data could be easily obtained by placing the end product on a PCB board connected with the labview controlled *I-V* measuring system. This system would be very efficient to use in a POC environment.

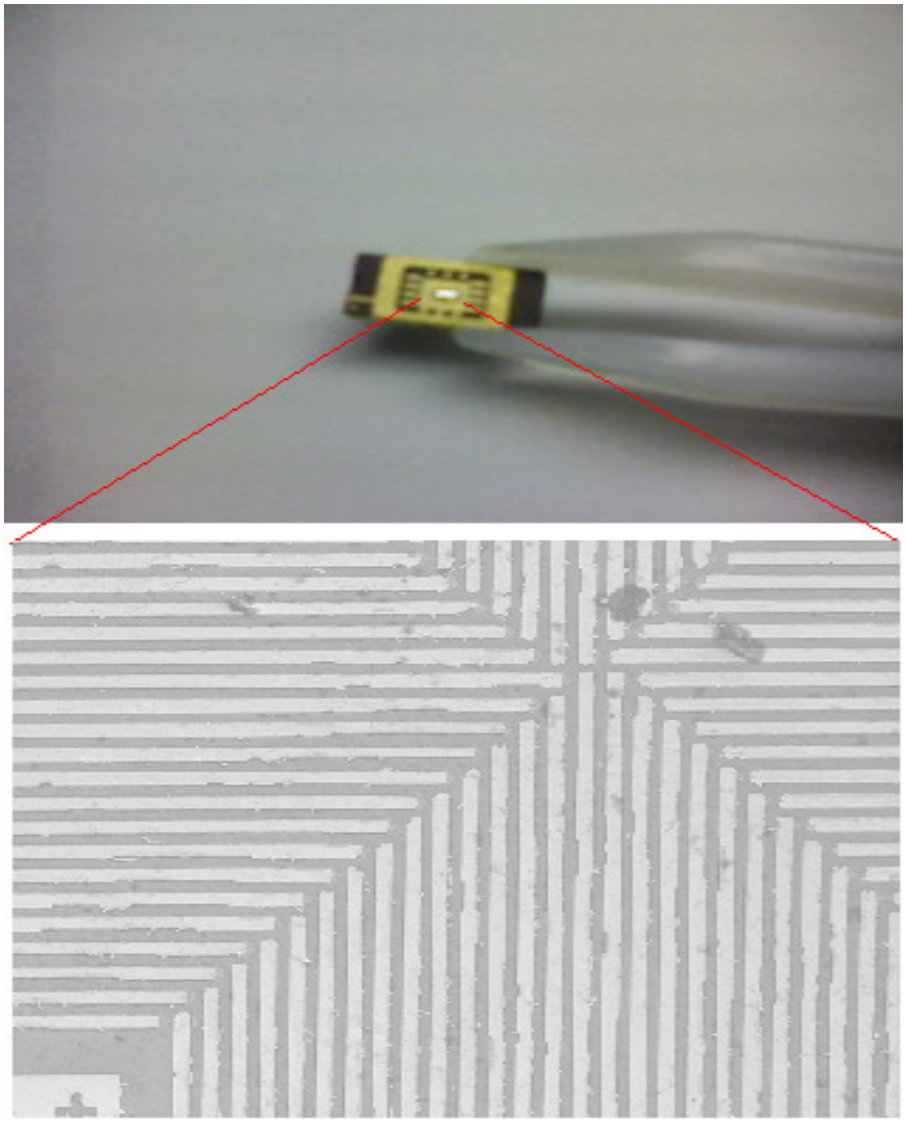

Figure-6.5: LDCC package mounted nanogap electrode chip.

APPENDIX A

DETAILED FABRICATION STEPS

Detailed Fabrication Steps

The nano-gap chip was fabricated in three main lithographic step and many sub steps in between. The detailed descriptions of the steps are as below:

Step – 1: E-beam lithography to pattern the first layer

In this step, nano-scale metal (Ti/Au) features would be deposited on the oxidized silicon wafer. For this purpose, the two layer mask was designed with help of IC Station software. This mask got two layers: the first one is for the nano-scale junctions and the second one for the thicker and micron scale probing pads. The mask software was then uploaded in the e-beam control software and appropriate procedures were followed to write the patterns on the wafer.

To pattern with e-beam, a special polymer or positive photo resist called PMMA was used. Since the intended metal thickness was only 150Å (50Å of Ti and 150Å of Au), the PMMA layer should not be thicker than 500Å. The PMMA photo resist and developer (M/I 1:1) was bought from MicroChem (Newton, MA) and I used their proprietary spin speed curve to figure out the RPM needed to put 500Å thick layer.

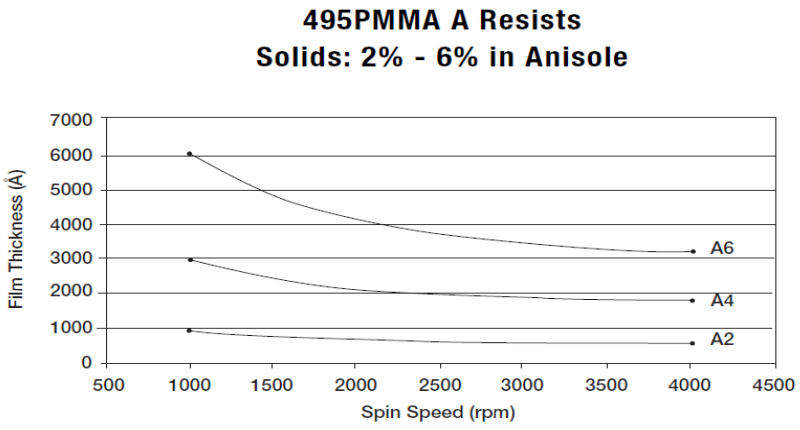

Figure A-1: The spin speed curve of 495-A type PMMA photo resist [70].

The detailed step by step process flow of e-beam lithography is given below:

1. Put the wafer in the spin coater and cover the wafer completely with PMMA. Program the spin coater with a ramp of 500 rpm/sec and final rpm of 4500 for 45 seconds.
2. Pre bake the PMMA coated wafer in a hot plate at 180 degree C for 90 seconds.
3. Put the wafer in e-beam machine and set the following parameters: Dose - 150 $\mu C/cm^2$; Energy – 30 KV. Let the software run until it's done, and then take the wafer out of the e-beam machine for development.
4. Develop the wafer in M/I 1:1 developer at 21 degree C (ideally) for 30 seconds.
5. Immerse the wafer in DI water for couple of minutes, and then rinse again with DI water.
6. Blow dry the wafer with N_2 gas.
7. Postbake: Optional.

After the above process is done, the wafer needs to be inspected under a optical microscope to make sure all the process went right and the etched part on the PMMA has the desired structures.

Step-2: E-beam evaporation to deposit Ti/Au

In this step, an e-beam evaporator was used to deposit 50 Å of Ti and 150 Å of Au on the PMMA patterned wafer. Figure 31 shows the AJA thin film deposition machine. AJA e-beam evaporator uses a high intensity beam of electron, with energy up to 30 KeV, to evaporate the desired metals. The wafer was mounted facing down above the source and rotated with a certain RPM to ensure uniform coverage. In some cases, substrate heater was used to heat the wafer to improve adhesion and uniformity of the evaporated material. The main evaporation chamber stays under high vacuum during the evaporation process to increase the *mean free path*. The average distance a molecule travels before colliding with another molecules is known as the *mean free path* (λ)of that molecule.

The *mean free path* is defined by:

$$\lambda = KT/\sqrt{(2\pi\, pd^2)}$$

where d is the diameter of the gas molecule (usually argon) and in the range of 2 to 5Å.

The detailed step by step process is given below:

1. Load the wafer in the loading chamber and turn the Rough/Turbo pump on. Wait for 1 hour and 30 minutes until you the pressure is 5 x 10^{-6} mbar in the loading chamber.
2. Open the load lock gate valve and load the wafer in the main evaporation chamber.
3. Set the substrate rotation at 50 rpm.
4. Select the first material: Ti from the material selector.
5. Reset the quartz crystal by zeroing the thickness monitor. Then select the appropriate metal density and impedance.
6. Do no turn the e-bema gun on until the main chamber pressure is 5 x 10^{-8} Torr.
7. Turn the e-beam gun ON .
8. Open all the shutters.
9. Deposit 50Å of Ti, and then close all the shutters.
10. Now select Au from the material selector.
11. Reset the quartz crystal by zeroing the thickness monitor. Then select the appropriate metal density and impedance.
12. Turn the e-beam gun ON.
13. Open all the shutters.
14. Deposit 150Å of Au, and then close all the shutters.

After the above steps were done, the whole wafer was immersed in acetone and left overnight to perform the lift-off process. At the end of the lift-off process, the wafer was put in ultrasonicator bath for 10 seconds to get rid of all the unwanted metal on top of the PMMA resist. The structures on the first layer should look like the following:

After the visual inspection the thickness of the first layer was measured with the help of a contact surface profilometer. A stylus was used to profile the contact surface.

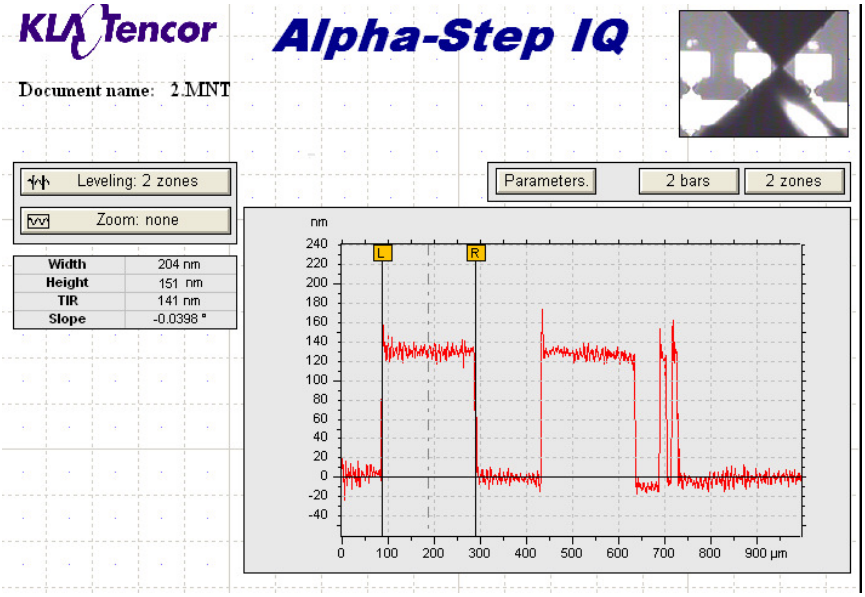

Figure A-2: A typical profilometer data showing the thickness of the measured first layer.

Step-3: Photolithography to pattern the second layer

In this step, conventional photolithography was done on top of the fabricated first layer to pattern the second probing pad layer. For photolithography, a dark field chrome mask was made earlier. This mask got the same layer-2 of the first e-beam mask. On the first layer, appropriate alignment marks were fabricated to align the second mask. A 5 inches mask was used with 450 nm UV light source. A different thicker photo resist called S1813 was used with MF-319 developer. The intended probing pad thickness was 600Å; 100Å of Ti and 500Å of Au. Thus, a thicker photoresist layer of 1000Å was deposited.

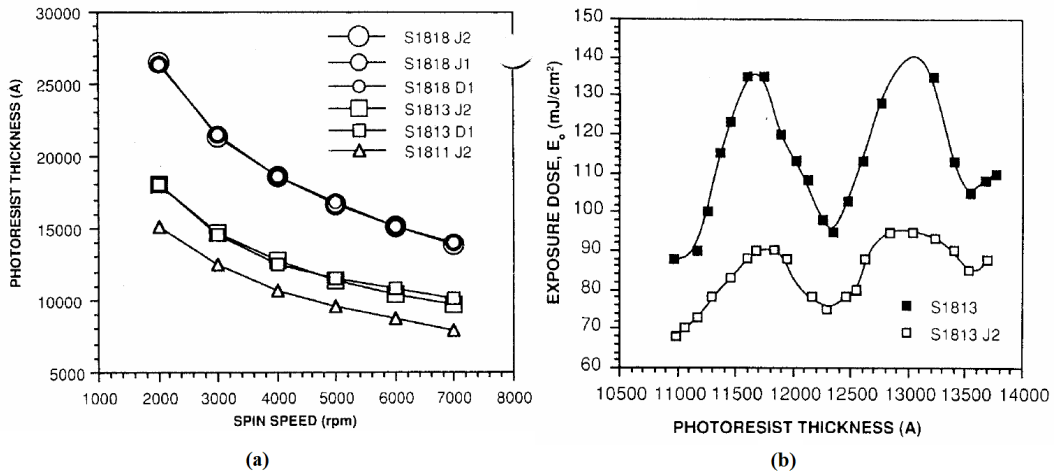

(a) (b)

Figure A.3: (a) Spin speed curve and (b) light interference curve for photoresist S1813[71]. The photoresist thickness was determined from the S1813 spin speed curve

The UV exposure time was calculated from light interference curve putting the resist thickness of 1000Å. For different spin speed, and eventually different thickness, the exposure energy should be derived from figure-33(b).

The detailed step by step process flow is given below:

1. Put the wafer in the spin coater and cover the wafer completely with S1813. Program the spin coater with a ramp of 500 rpm/sec and final rpm of 5000 for 60 seconds.
2. Pre-bake the S1813 coated wafer in a hot plate at 115 degree C for 60 seconds.
3. Put the optical mask in the mask aligner in appropriate position. Then put the wafer. Set the exposure time to 8.5 seconds and expose.
4. Develop the exposed wafer in MF-319 type developer at room temperature for 45 seconds.
5. Immerse the wafer in DI water for couple of minutes, and then rinse again with DI water. Then blow dry the wafer with N_2 gas. No post bake needed.

After the entire above step were done, the wafer should have big opening in the photoresist to deposit the second layer of Ti/Au.

Step-4: E-beam evaporation to deposit second layer probing pads

In this step, another e-beam evaporator called CHA was used to deposit thick layer of Ti/Au probing pads.

The detailed step by step process is given below:

1. Check the water pump in the back of CHA
2. Turn the mechanical pump on.
3. After 20 minutes, switch off the “FORE” switch and turn the “CRYO” pump on. The cryo pump should start from 50 mTorr and the temperature gauge should read 300K
4. Wait for 1 hour and 30 minutes.
5. Load the wafer in the planetary above.
6. Load two crucibles contain Ti and Au in appropriate places.
7. Reset the quartz crystal by zeroing the thickness monitor.
8. Lower the bell jar and wait till it reaches 5×10^{-6} Torr.
9. Turn the power supply on and adjust the e-beam right in the middle of the crucible.
10. Open all the shutters.
11. Deposit 100Å of Ti.
12. Press the automatic switch to move multiple crucible holders. Make sure the crucible with Au is in the right place.
13. Turn the power supply on and adjust the e-beam right in the middle of the crucible.
14. Deposit 600Å of Au.
15. Turn the power supply off and close all the shutters.
16. Vent the bell jar and take the wafer out.

After all the above steps were done, follow exactly the step-3: leave the wafer immersed in acetone all night to perform the lift-off process. At the end of the lift-off process, the wafer was put in ultrasonicator bath for 10 seconds to get rid of all the unwanted metal on top of S1813 resist.

APPENDIX B

DETAILED DNA ATTACHMENTS PROCEDURES

Detailed DNA Attachment procedures

The detailed step by step attachment chemistry is given below:

1. All three chips were cleaned with oxygen plasma at 200W in $Ar+O_2$ gas. The purpose of oxygen plasma is to make the silicon dioxide hydrophilic, which introduces OH group to the oxide surface.
2. Clean the chips with Piranha solution clean. Piranha cleaning removes all the unwanted particles from the surface making it super clean.
3. The chips were rinsed with deionized water and dried with abundance of N_2 gas.
4. The chips were then put in a nitrogen glove box with controlled ambience and temperature and rest of the attachment process was carried on over there.
5. Make a solution containing 5% Aminopropyltrimethoxysilane (APTMS) solution with 95% ethanol. Immerse the chips in this solution for 12 hours.
6. Wash the chips with ethanol and DI water.
7. Heat the chips at 110 ℃ for 15 minutes in a fan-operated oven.
8. Immerse the chips in 1 mM 1,4-Phenylene diisothiocyanate (PDITC) dissolved in dimethylformamide (DMF) containing 10% pyridine for 24 hours. To make 1 mM PDITC solution: Stock PDITC solution concentration: 20 mM. To get 1 mM concentration, the following formula was used: $m_1v_1 = m_2v_2$

   20 mM x X = 10 ml x 1mM; solving for, X = 0.5 ml.

   So for 10ml of PDITC: Take 500 µl from stock PDITC solution.

   10% pyridine → 10% of 10 ml = 1 ml.
9. Wash the chips with DMF and 1,2-dichloroethane and dry with nitrogen.
10. Make the probe DNA solution: To make the probe DNA solution:

    The stock DNA concentration is 100 pmol/ µl. To make 2 pmol/ µl concentration of 6 ml solution, same formula was used: $m_1v_1 = m_2v_2$

    100 pmol/ µl x X = 2 pmol/ µl x 6 ml. Solving for X = 0.12 ml or 120 µl.

Then immerse each chip in 40 µl of this solution and incubate for 72 hours at 37℃.

11. Wash the chips with DI water and ethanol, then dry with nitrogen gas.
12. Heat the chip along with surface attached probes three times to ensure all molecule forms a hairpin loop structure.
13. Make the blocking solution. Blocking solution is needed to deactivate the unreacted surface-bound isothiocyanate groups. Approximately 9 ml of blocking solution is required for three chips. The blocking solution is consist of 50 mM 6-amino-1-hexanol and 150 mM DPEA in DMF. Immerse the chips in blocking solution for 12 hours.
14. Wash the chips with DMF, Ethanol and DI water.
15. Make the PC target DNA and MM target DNA solution. This part is very important because both the target concentration is 2 fmol/µl. This femto molar concentration will show how sensitive this DNA sensor is compared to others. To make 2 femto molar concentration DNA solution: 5ml of solution is required for each PC and MM chip. The molar concentration of stock DNA is 2pmol/µl. using the previously used formula: $m_1v_1 = m_2v_2$,2pmol/µl x X = 2 fmol/µl x 5 ml; Solving for, X = 5 µl. Mix this 5µl solution with 5 ml of TRIS EDTA buffer solution. Repeat this exact same step for both PC and MM DNA solution.
16. Immerse the PC chip in PC target and MM chip in MM target DNA solution for 24 hours at 40℃.
17. Wash the chips with ethanol and DI water.
18. Make the GNP reporter DNA solution. For this purpose, 100 nm Au nanoparticles were used. GNP reporter DNA was synthesized by derivatizing 5 mL of an aqueous 100 nm diameter Au nanoparticle solution of 17nM concentration. After incubating for 16 h, the solution was brought to 0.1 M NaCl, 10 mM phosphate buffer (pH 7) and allowed to stand for 40 h. The process then followed by centrifugation for at least 25 min at 14 000 rpm to remove excess reagents. After the removal, the red oily precipitate was washed

with 5 mL of a stock 0.1 M NaCl, 10 mM phosphate buffer (pH 7) solution, recentrifuged, and redispersed in 5 mL of a 0.3 M NaCl, 10 mM phosphate buffer (pH 7), 0.01% azide solution.

19. Immerse all three chips in GNP reporter DNA solution and incubate at 4 ℃ for 24 hours.
20. Wash the chip with cold DI water and dry with N_2 gas.

REFERENCES

1. D. D. Eley, a.D.I.S., *Semiconductivity of Organic Substances.* Trans. Faraday Soc, 1962. **58**.
2. Yoo, K.H., et al., *Electrical conduction through poly (dA)-poly (dT) and poly (dG)-poly (dC) DNA molecules.* Physical Review Letters, 2001. **87**(19): p. 198102.
3. Drummond, T.G., M.G. Hill, and J.K. Barton, *Electrochemical DNA sensors.* Nature biotechnology, 2003. **21**(10): p. 1192-1199.
4. Ratner, M.A. and A. Aviram, *Molecular rectifiers.* Chem. Phys. Lett, 1974. **29**: p. 277–283.
5. Fink, H.W. and C. Schönenberger, *Electrical conduction through DNA molecules.* Nature, 1999. **398**(6726): p. 407-410.
6. Adessi, C., S. Walch, and M.P. Anantram, *Environment and structure influence on DNA conduction.* Physical Review B, 2003. **67**(8): p. 81405.
7. Porath, D., et al., *Direct measurement of electrical transport through DNA molecules.* Nature, 2000. **403**(6770): p. 635-637.
8. Hwang, J.S., et al., *Electrical transport through 60 base pairs of poly (dG)-poly (dC) DNA molecules.* Applied Physics Letters, 2002. **81**: p. 1134.
9. Xu, B., et al., *Direct conductance measurement of single DNA molecules in aqueous solution.* Nano letters, 2004. **4**(6): p. 1105-1108.
10. Iqbal, S.M., et al., *Direct current electrical characterization of ds-DNA in nanogap junctions.* Applied Physics Letters, 2005. **86**: p. 153901.
11. Owa, S., et al. *Immersion Lithography Ready for 45 nm Manufacturing and Beyond*. 2007.
12. Balzani, V., A. Credi, and M. Venturi, *The bottom-up approach to molecular-level devices and machines.* CHEMISTRY-WEINHEIM-EUROPEAN JOURNAL-, 2002. **8**(24): p. 5524-5532.
13. Hand, A., *Litho simulation: Enables the leading edge.* Semiconductor international, 2006. **29**(8).
14. Cahill, D.G., et al., *Nanoscale thermal transport.* Journal of Applied Physics, 2003. **93**: p. 793.
15. Feynman, R., *There's plenty of room at the bottom, 1959.* J. Microelectromech. Syst, 1992. **1**: p. 60–66.
16. Li, X.L., et al., *Measurement of electron transport properties of molecular junctions fabricated by electrochemical and mechanical methods.* Surface Science, 2004. **573**(1): p. 1-10.
17. Cui, X.D., et al., *Reproducible measurement of single-molecule conductivity.* Science, 2001. **294**(5542): p. 571.
18. Cui, X.D., et al., *Changes in the electronic properties of a molecule when it is wired into a circuit.* J. Phys. Chem. B, 2002. **106**(34): p. 8609-8614.
19. Xu, B. and N.J. Tao, *Measurement of single-molecule resistance by repeated formation of molecular junctions.* Science, 2003. **301**(5637): p. 1221.
20. Derycke, V., et al., *Carbon nanotube inter-and intramolecular logic gates.* Nano Letters, 2001. **1**(9): p. 453-456.
21. Bachtold, A., et al., *Logic circuits with carbon nanotube transistors.* Science, 2001. **294**(5545): p. 1317.

22. Berlin, Y.A., A.L. Burin, and M.A. Ratner, *DNA as a molecular wire.* Superlattices and Microstructures, 2000. **28**(4): p. 241-252.
23. Nylander, C., *Chemical and biological sensors.* Journal of Physics E: Scientific Instruments, 1985. **18**: p. 736-750.
24. Chudy, M., et al., *Novel head for testing and measurement of chemical microsensors.* Analytica Chimica Acta, 2001. **429**(2): p. 347-355.
25. Yeo, W.H., et al. *Direct concentration of circulating DNA by using a nanostructured tip*. 2008.
26. Iijima, S. and T. Ichihashi, *Single-shell carbon nanotubes of 1-nm diameter.* 1993.
27. Tang, J., et al., *Assembly of 1D nanostructures into sub-micrometer diameter fibrils with controlled and variable length by dielectrophoresis.* Advanced Materials, 2003. **15**(16): p. 1352-1355.
28. Liu, Y.S., et al., *Electrical characterization of DNA molecules in solution using impedance measurements.* Applied Physics Letters, 2008. **92**: p. 143902.
29. Niu, S.Y., et al., *Nucleic acid biosensor for DNA hybridization detection using rutin–Cu as an electrochemical indicator.* Electrochimica Acta, 2009. **54**(5): p. 1564-1569.
30. Hong, J.W., et al., *Inside Front Cover: Conjugated-Polymer/DNA Interpolyelectrolyte Complexes for Accurate DNA Concentration Determination (Adv. Mater. 7/2006).* Advanced Materials, 2006. **18**(7).
31. Zhang, J., et al., *Sequence-specific detection of femtomolar DNA via a chronocoulometric DNA sensor (cds): effects of nanoparticle-mediated amplification and nanoscale control of DNA assembly at electrodes.* J. Am. Chem. Soc, 2006. **128**(26): p. 8575-8580.
32. Rakitin, A., et al., *Metallic conduction through engineered DNA: DNA nanoelectronic building blocks.* Physical Review Letters, 2001. **86**(16): p. 3670-3673.
33. Watanabe, H., et al., *Single molecule DNA device measured with triple-probe atomic force microscope.* Applied Physics Letters, 2001. **79**: p. 2462.
34. Cai, L., H. Tabata, and T. Kawai, *Self-assembled DNA networks and their electrical conductivity.* Applied Physics Letters, 2000. **77**: p. 3105.
35. Kasumov, A.Y., et al., *Proximity-induced superconductivity in DNA.* Science, 2001. **291**(5502): p. 280.
36. Moreland, J. and J.W. Ekin, *Electron tunneling experiments using Nb Sn "break"junctions.* Journal of Applied Physics, 1985. **58**: p. 3888.
37. Heurich, J., et al., *Electrical transport through single-molecule junctions: From molecular orbitals to conduction channels.* Physical review letters, 2002. **88**(25): p. 256803.
38. Park, H., et al., *Fabrication of metallic electrodes with nanometer separation by electromigration.* Applied Physics Letters, 1999. **75**: p. 301.
39. Morpurgo, A.F., C.M. Marcus, and D.B. Robinson, *Controlled fabrication of metallic electrodes with atomic separation.* Applied physics letters, 1999. **74**: p. 2084.
40. Zhou, C., et al., *Microfabrication of a mechanically controllable break junction in silicon.* Applied Physics Letters, 1995. **67**: p. 1160.
41. http://www.fzk.de/fzk/idcplg?IdcService=FZK&node=2341&lang=en. [cited.
42. Bezryadin, A. and C. Dekker, *Nanofabrication of electrodes with sub-5 nm spacing for transport experiments on single molecules and metal clusters.* Journal of Vacuum Science & Technology B: Microelectronics and Nanometer Structures, 1997. **15**: p. 793.
43. Bezryadin, A., C. Dekker, and G. Schmid, *Electrostatic trapping of single conducting nanoparticles between nanoelectrodes.* Applied Physics Letters, 1997. **71**: p. 1273.
44. Núñez, M.E., D.B. Hall, and J.K. Barton, *Long-range oxidative damage to DNA: effects of distance and sequence.* Chemistry & Biology, 1999. **6**(2): p. 85-97.

45. Endres, R.G., D.L. Cox, and R.R.P. Singh, *Colloquium: The quest for high-conductance DNA.* Reviews of modern physics, 2004. **76**(1): p. 195-214.
46. Storm, A.J., et al., *Single Molecule Experiments On DNA With Novel Silicon Nanostructures*. 2004, IOS Press, Incorporated.
47. Lee, H.Y., et al., *Control of electrical conduction in DNA using oxygen hole doping.* Applied Physics Letters, 2002. **80**: p. 1670.
48. Hwang, J.S., S.W. Hwang, and D. Ahn, *Electrical conduction measurement of thiol modified DNA molecules.* Superlattices and Microstructures, 2003. **34**(3-6): p. 433-438.
49. De Pablo, P.J., et al., *Absence of dc-Conductivity in -DNA.* Physical review letters, 2000. **85**(23): p. 4992-4995.
50. Braun, E., et al., *DNA-templated assembly and electrode attachment of a conducting silver wire.* Nature, 1998. **391**(6669): p. 775-778.
51. Hipps, K.W., *Molecular electronics: it's all about contacts.* Science, 2001. **294**(5542): p. 536.
52. Gorringe, K.L., et al., *High-resolution single nucleotide polymorphism array analysis of epithelial ovarian cancer reveals numerous microdeletions and amplifications.* Clinical Cancer Research, 2007. **13**(16): p. 4731.
53. Futreal, P.A., et al., *A census of human cancer genes.* Nature reviews. Cancer, 2004. **4**(3): p. 177.
54. Etzioni, R., et al., *The case for early detection.* Nature Reviews Cancer, 2003. **3**(4): p. 243-252.
55. Zhang, J., et al., *A gold nanoparticle-based chronocoulometric DNA sensor for amplified detection of DNA.* Nature Protocols, 2007. **2**(11): p. 2888-2895.
56. Mikkelsen, S.R., *Electrochemical biosensors for DNA sequence detection.* Electroanalysis-Weinheim, 1996. **8**(1): p. 15-19.
57. Willner, I. and M. Zayats, *Electronic aptamer-based sensors.* ANGEWANDTE CHEMIE-INTERNATIONAL EDITION IN ENGLISH-, 2007. **46**(34): p. 6408.
58. Wei, F., et al., *Achieving differentiation of single-base mutations through hairpin oligonucleotide and electric potential control.* Biosensors and Bioelectronics, 2003. **18**(9): p. 1149-1155.
59. Jin, Y., et al., *Hairpin DNA probe based electrochemical biosensor using methylene blue as hybridization indicator.* Biosensors & bioelectronics, 2007. **22**(6): p. 1126-1130.
60. Huncharek, M., J. Muscat, and J.F. Geschwind, *K-ras oncogene mutation as a prognostic marker in non-small cell lung cancer: a combined analysis of 881 cases.* Carcinogenesis, 1999. **20**(8): p. 1507.
61. Bos, J.L., et al., *Prevalence of ras gene mutations in human colorectal cancers.* Nature, 1987. **327**(6120): p. 293-297.
62. Burnet, F.M., *The concept of immunological surveillance.* Progress in experimental tumor research. Fortschritte der experimentellen Tumorforschung. ProgrÃ¨ s de la recherche expÃ© rimentale des tumeurs, 1970. **13**: p. 1.
63. Trahey, M. and F. McCormick, *A cytoplasmic protein stimulates normal N-ras p21 GTPase, but does not affect oncogenic mutants.* Science, 1987. **238**(4826): p. 542.
64. Gorshkova, E.V., et al., *Codon 12 region of mouse K-ras gene is the site for in vitro binding of transcription factors GATA-6 and NF-Y.* Biochemistry (Moscow), 2005. **70**(10): p. 1180-1184.
65. www.generunner.ne.
66. Storhoff, J.J., et al., *One-pot colorimetric differentiation of polynucleotides with single base imperfections using gold nanoparticle probes.* J. Am. Chem. Soc, 1998. **120**(9): p. 1959-1964.

67. Wang, W., T. Lee, and M.A. Reed, *Mechanism of electron conduction in self-assembled alkanethiol monolayer devices.* Physical Review B, 2003. **68**(3): p. 35416.
68. John G. Simmons, *Generalized Formula for the Electric Tunnel Effect between Similar Electrodes Separated by a Thin Insulating Film.* J. Appl. Phys, 1963. **34**: p. 1793.
69. www.spectrum-semi.com.
70. http://www.microchem.com/products/pdf/PMMA_Data_Sheet.pdf.
71. http://cmi.epfl.ch/photo/photo_process/files/Data_S1800.pdf.

BIOGRAPHICAL INFORMATION

Mohammud Noor is a Bangladeshi citizen doing his Masters in Electrical Engineering and will be done with his degree in December of 2009. He also did his BS in Electrical Engineering, also from UTA in 2005. He is an avid video gamer and likes to travel at the speed of (close to) light. Cricket, NBA, NFL, Music and Movies are some of his favorite pastimes. He likes Nirvana, Alice in chains, Tool, Pearl Jam, Dream Theatre, Iron Maiden, Metallica, Warfaze, Dolchut and many more. The top five of his favorite movies are Forest Gump, Jerry Mcguire, Count of Monte Cristo, Shawshank Redemption and Shimana Periya.

He has immense interest on Micro Electro Mechanical Systems (MEMS) and Nanotechnology. He plans to continue his research on disease diagnostics in future and desire to have a career in this field. He has expertise on Scanning electron Microscope, FIB/E-beam Lithography, Oxidation/Diffusion, Optical Lithography, Probe Station and Semiconductor Parameter Analyzer, E-Beam Evaporation, PECVD, LPCVD, Sputtering, RIE/DRIE, Profilometer, Ellipsometer and Wire Bonder, among many other things.